Volcanic rifting at Martian grabens

Daniel Mège,[1] Anthony C. Cook,[2,3] Erwan Garel,[4] Yves Lagabrielle,[5] and Marie-Hélène Cormier[6]

[1]   A large fraction of surface extension on Mars occurred at segmented grabens having width/length ratios akin to oceanic rifts on Earth. Association with volcanic landforms such as pit craters clearly suggests interconnection between tectonic and magmatic processes. A Martian rift evolution model is proposed on the basis of new geomorphological and structural interpretations of imagery, high-resolution digital elevation models (DEMs), scaled experimental modeling and three-dimensional boundary element modeling of magmatic and tectonic processes, and a comparison with terrestrial rifts. The DEMs were obtained from Mars Observer Laser Altimeter, Viking Orbiter stereo images, or a combination of both. Comparison of terrestrial rifts included Afar, Iceland, and the East Pacific Rise. The ambient extensional stress field induced by regional body forces is combined at depth with decompression melting and mantle plume thermal anomaly, resulting in emplacement of elongated magma reservoirs along the grabens. Injection of dikes above the reservoirs and flood basalt eruption result in a reservoir underpressurization of up to hundreds of MPa and induces surface collapse. Each collapse event is associated with an eruption of volcanic volumes akin to those of individual flow eruptions in large terrestrial igneous provinces. The geometry and mechanisms of graben formation and surface collapse are described and used to infer reservoir depth and width. We conclude from this study that giant dike swarms akin to typical giant terrestrial dike swarms are unlikely to underlie the volcanic Martian grabens on the basis one graben-one dike. Rather, every volcanic graben segment appears to own a local dike swarm perhaps analogous to the dike swarms in the Icelandic fissure zones.   *INDEX TERMS:* 5475 Planetology: Solid Surface Planets: Tectonics (8149); 5480 Planetology: Solid Surface Planets: Volcanism (8450); 6225 Planetology: Solar System Objects: Mars; 8121 Tectonophysics: Dynamics, convection currents and mantle plumes; 8010 Structural Geology: Fractures and faults; *KEYWORDS:* rifting, graben, pit crater, magma chamber, dyke

1. Introduction

[2] Many Martian narrow grabens display collapse features. This paper provides a short review of mechanisms of narrow graben formation and discusses evidence that the collapse features have a volcanic origin. We call narrow grabens that have been altered by further collapse modified grabens. Modified grabens include grabens associated with catenae as well as other depression types. Relationships between graben formation and magmatic processes are explored. The influence of dike emplacement (driving pressure during dike propagation, pressure drop during withdrawal or freezing) in graben geometry and in the formation of pit craters and other depressions is discussed. Deeper processes such as magma chamber compaction and withdrawal are then investigated. A qualitative model of tectonic extension simultaneous to magma emplacement at depth is presented, and quantified using morphometric analysis of collapse depressions, experimental modeling, and numerical modeling of magmatic deflation.

1.1. Martian Narrow Grabens

[3] Mars, Venus and the Moon all display so-called "narrow grabens" [e.g., *Golombek*, 1979], typically 2–5 km in width and hundreds or thousands of km in length (Figure 1). Earlier photoclinometric studies have shown that in the Syria Planum-Valles Marineris area their depth is commonly less than 100 m to a few hundred meters [*Tanaka*

[1]Laboratoire de Tectonique, Université Pierre et Marie Curie, Paris, France.
[2]Center for Earth and Planetary Studies, Smithsonian Institution, Washington, D. C., USA.
[3]Now at School of Computer Science and Information Technology, University of Nottingham, Nottingham, UK.
[4]Laboratoire de Géodynamique des Rifts et des Marges Passives, Université du Maine, Le Mans, France.
[5]Institut de Recherche pour le Développement, Université de Bretagne Occidentale, Plouzané, France.
[6]Lamont-Doherty Earth Observatory, Columbia University, Palisades, New York, USA.
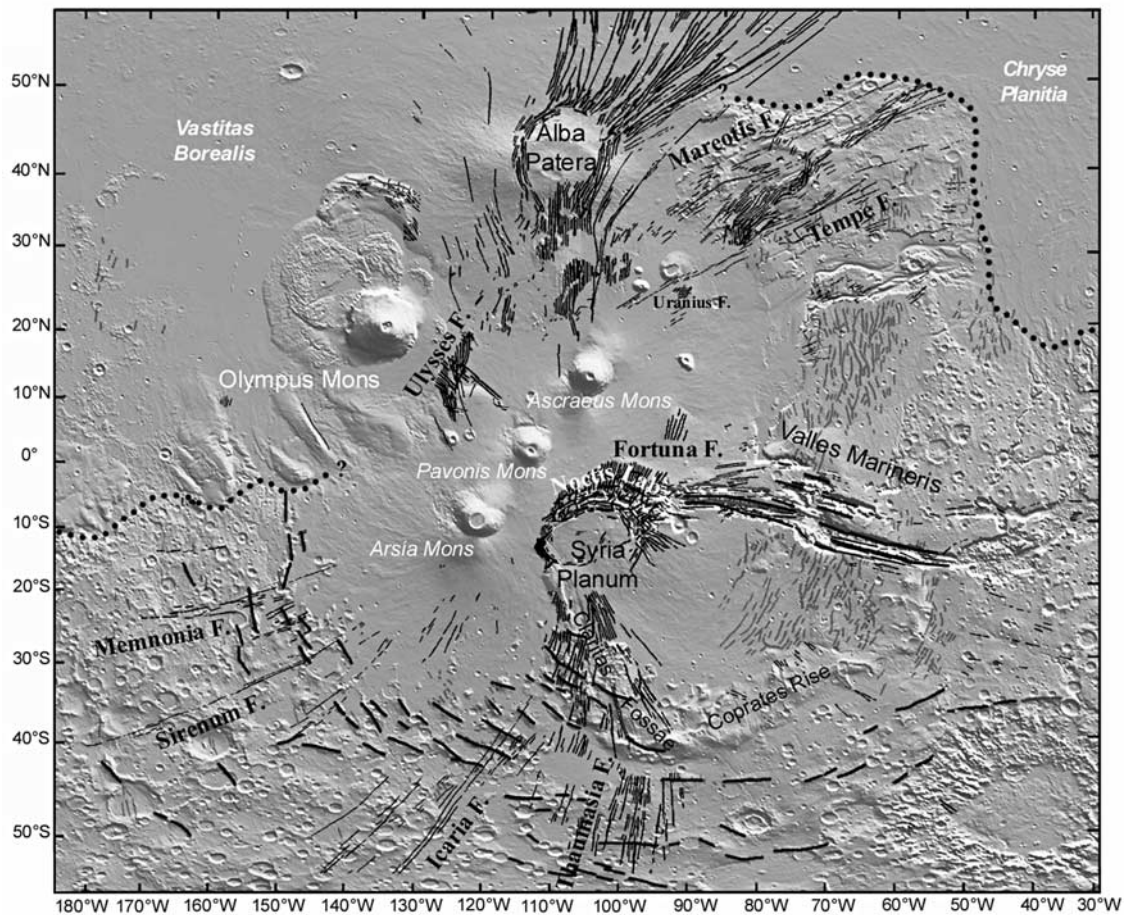
Figure 1. Structural map of the Tharsis region. Thin black lines: grabens (fossae); thick black lines with barbules: main visible faults of the Valles Marineris canyon system; other thick black lines: South Tharsis ridge as mapped by *Mège and Ernst* [2001] using MGS/MOLA topography data; gray lines: wrinkle ridges as defined by *Watters* [1993]. The dotted line shows the location of the dichotomy boundary.

and Davis, 1988]. These values are probably representative of most Martian narrow grabens as well as Venusian and narrow lunar grabens. Typical narrow grabens are bounded by two parallel segmented border faults, and do not usually display additional structures at common Viking Orbiter image resolution (20–100 m/pixel) such as transfer faults except in areas where previous oblique fracturing has induced greater complexity, such as at Tantalus Fossae [*Tanaka*, 1990]. At MOC image scale (1–10 m/pixel) typical narrow grabens such as Thaumasia, Uranius, and Ceraunius Fossae display structural complexity similar to terrestrial grabens, which suggests that the frequently used term simple graben should be avoided (Figure 2). However, no significant transcurrent movement has been detected in areas where lava flows are offset by narrow graben border faults.

[4] Models of narrow graben formation have attempted to account for several features that were thought to be atypical of terrestrial grabens. Because of the lack of accurate digital elevation models (DEMs) prior to the availability of Mars Observer Laser Altimeter (MOLA) data, image analysis had suggested that narrow graben border faults have symmetric vertical offset. From this viewpoint, the Canyonlands grabens, Utah, were long thought to be a good (maybe the only)

example of terrestrial planetary narrow grabens. Ad hoc narrow grabens models were derived from this example in which an evaporite layer has been thought to play a key role in the mechanics of faulting [*McGill and Stromquist*, 1979]. Examination of MOLA altimetry data and detailed structural analysis has shown however that neither planetary narrow grabens [*Schultz et al.*, 2000] nor the Canyonlands grabens [*Schultz and Moore*, 1996] display symmetric border faults. *Schultz et al.* [2000] propose an hourglass model consistent with other terrestrial examples. At broader scale, strong similarity exists between narrow graben structure and the structure of typical continental terrestrial rifts such as the Rhine graben and the Gregory rift (D. Mège, unpublished).

[5] The very high graben length-depth ratio, on the order of 10^5, was also considered to be a feature characteristic of graben tectonics at extraterrestrial solid bodies, although slow and intermediate spreading centers on Earth also display such a feature. *Schultz and Fori* [1996] and *Schultz* [1997, 2000] have shown that usual terrestrial fault displacement length scaling applies if fault linkage is taken into account. They concluded that graben length is not a strong mechanical issue and merely requires a steady stress source acting over large surface area. Several hypotheses have been proposed for explaining the very low narrow
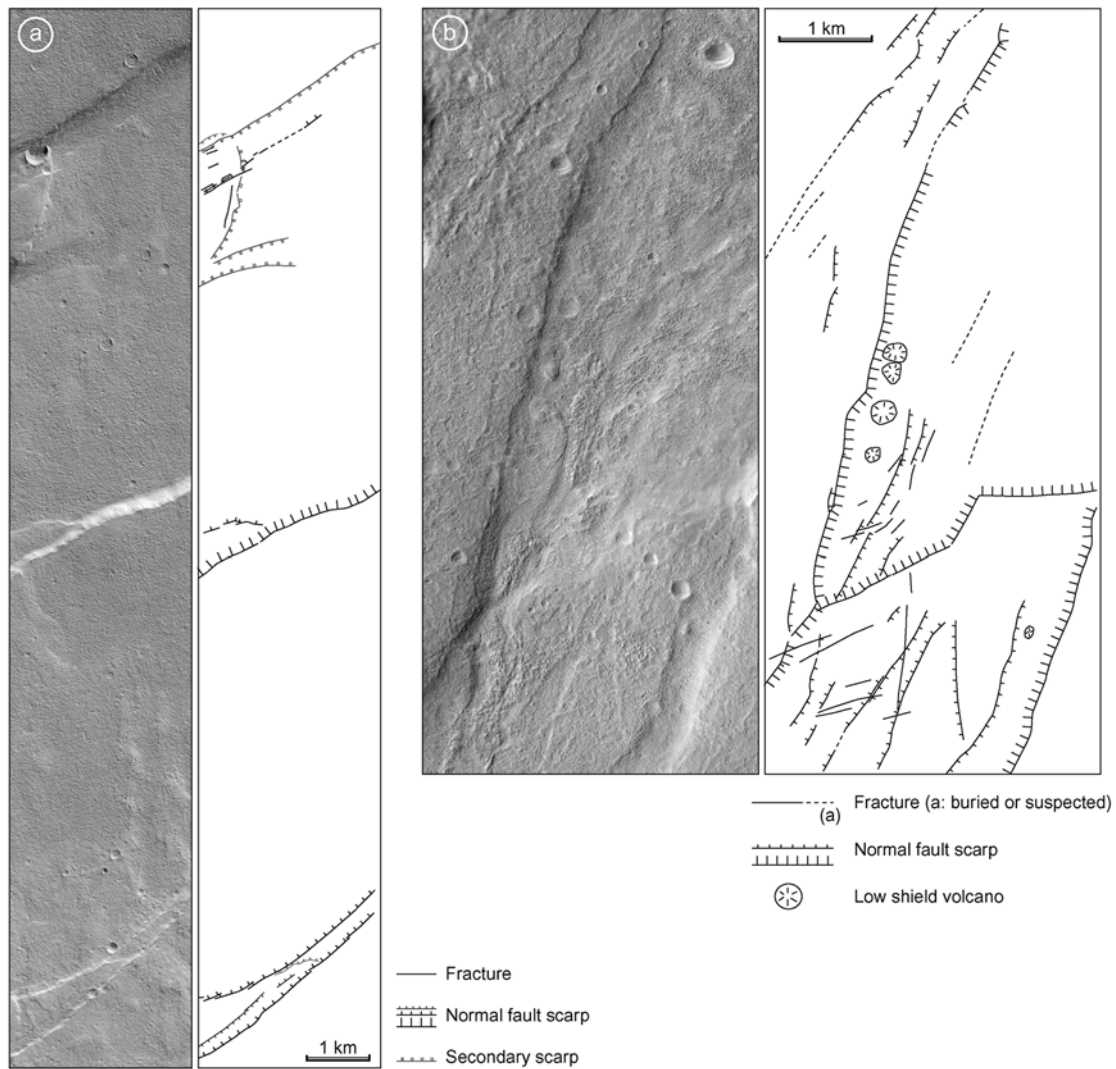
Figure 2. High-resolution views of narrow grabens. (a) Typical narrow graben at Alba Fossae, northwest of Alba Patera. Note that the northern rim of the impact crater at the northern border fault scarp was cut by the border fault and subsequently buried, which is evidence of postfaulting mass wasting at the border fault. In this example, postfaulting mass wasting may explain the absence of along-strike variation of fault displacement. MOC image M09-06510 centered at 112.35°W, 45.49°N, 6.21 m/pixel. (b) Typical narrow graben at Thaumasia Fossae. Low shield volcanoes are aligned along the western graben border fault. Although major collapse features are not observed within the graben, local collapse occurred at summit calderas (<50 m diameter), suggesting volcanic activity contemporaneous with tectonic extension. MOC image M00-00991 centered at 95.31°W, 43.96°N, 2.76 m/pixel. MOC images by NASA/JPL/MSSS. The coordinates given in the figure captions refer to the MGS/MOLA datum for MOC images and Viking datum for Viking images.

graben width-length ratio, on the order of $10^{-3}-10^{-2}$. *Tanaka and Golombek* [1989] proposed that narrowness results from existence of deep tension fractures whose upper termination would correspond to a rheological interface such as a permafrost layer or the base of a megaregolith, where V-shaped grabens would have initiated and propagated toward the surface. Model assessment is made difficult by apparent lack of terrestrial analogs. However, mechanically the maximum depth a tension fracture can reach before it turns into a fault on Mars, even under high fluid pressure conditions, cannot exceed 1 or 2 km [e.g., *Mège and Masson*, 1997]. This corresponds to a fracture length that can hardly exceed several kilometers, and is therefore too small to explain planetary narrow graben length. *Melosh and Williams* [1989] advocated that slip along a single fault in elastic medium may generate a compression zone at depth that locks the fault and induces nucleation of an antithetic fault at a short distance from the first fault. This model requires that the crust be intact before the graben forms, and that the extension rate be low enough not to annihilate the compression at the bottom of the first fault after slip. This is necessary in order to make the nucleation of another fault necessary instead of continuing slip along the first fault. The most recent hypothesis has

been that the small width-length ratio results from strain concentration at the surface above nonfeeder dikes either in response to magma pressure or density and strength contrast with the host rock [*Schultz*, 1988; *Tanaka et al.*, 1991; *Mège and Masson*, 1996]. A reason why large strain was achieved by the formation of many narrow graben swarms instead of by the growth of a few major grabens, may also be that the narrow grabens formed above corresponding giant dikes, similar to the dikes in terrestrial giant mafic swarms. Earlier, *Wise* [1976] had suggested that strain distribution might be a consequence of the existence of a shallow ductile layer below the grabens.

[6] The steady broad-scale stress sources required for narrow graben development are likely to have originated from the magmatic activity and lithosphere loading by the Tharsis and Elysium volcanic provinces. *Merle and Borgia* [1996] showed that uplift of volcanic topography generates body forces inducing gravitational spreading of the topography, resulting in the development of radiating grabens from the central region to the lower uplift flank. They also showed that graben width and spacing depends on the brittle/ductile crust ratio. Furthermore, *Van Wyk de Vries and Merle* [1996] showed that topographic building in an extensional remote stress field results in long and narrow grabens extending from the summit of the uplift to the most remote areas in which the same remote stress field exerts, which is pretty much the case for many narrow grabens around the Tharsis and Elysium volcanic shields. Stress modeling of the whole Tharsis magmatic load (including both the topographic load and the accreted magmatic materials) was shown to reproduce part of the radiating extensional patterns in some detail [*Banerdt and Golombek*, 2000]. Other possible contributing regional stress sources include plume-induced uplift [*Mège*, 2001] and overpressure in huge central magma chambers in the Tharsis and Elysium regions [*Mège and Masson*, 1996].

1.2. Modified Grabens, Pits, and Troughs

[7] Narrow grabens are frequently associated with aligned collapse depressions, and occasionally with positive relief of volcanic origin including lava flows, cinder cones, spatter cones, small shield volcanoes, and spatter ridges [*Cattermole*, 1986, 1992; *Davis et al.*, 1995; *Mège and Masson*, 1996]. Frequently the depressions have partly or wholly removed the narrow graben border faults, and are associated with newly formed fractures.

[8] Modified grabens are mostly distributed at and around the large Tharsis and Elysium volcanic shields, and in most regions on Mars that were deformed in extension. Figure 3 shows typical relationships observed between narrow grabens and modified grabens at Tempe Terra, Elysium Fossae, and southeast of Valles Marineris. At a first approximation, the depressions include:

[9] (1) pits and pit chains (Figure 4a) and elongated U-shaped troughs of similar depth aligned with the pits (Figure 4b). Alignments of pits and elongated U-shaped troughs make catenae, a planetary term first used by *Antoniadi* [1930] to name albedo features and redefined from 1973 to mean crater chains, many of which are associated with a graben.

[10] (2) shallow flat-floored depressions (Figure 4c), usually in areas where pits are also observed. Some shallow flat-floored depressions are ovoid (many examples are found at Tempe Terra) while the others have a marked linear trend (e.g., Elysium Chasma area).

[11] (3) linear U-shaped troughs (Figure 4d). The difference made here with elongated U-shaped troughs is based on length. Linear U-shaped troughs are wider than grabens in the same area and have monotonous U-shaped wall morphology displaying no evidence of faulting for lengths frequently greater than 100 km.

[12] (4) small chasmata, such as part of the Elysium Fossae (Figure 4e) and the chasmata aligned with pit chains parallel to the main Valles Marineris grabens. Small chasmata are wider and deeper than U-shaped troughs (e.g., Elysium Chasma depth is some 2 km deep [*MOLA Science Team*, 1997]).

[13] Collapse features are either observed within narrow grabens, laterally connected to narrow grabens, or aligned parallel to narrow grabens but with no apparent connection at surface. In the latter case, either graben fault scarp collapse occurred along the whole graben, or a narrow graben never formed, meaning that narrow graben formation and U-shaped trough formation may result from the same process but without any causal link.

1.2.1. Pits and Pit Chains

[14] Pits and coalescing pits have been interpreted as pit craters formed by pressure drop above dikes [*Cattermole*, 1992; *Davis et al.*, 1995; *Mège and Masson*, 1996; *Liu and Wilson*, 1998; *Scott et al.*, 2000], and in a few locations as maars [*McGetchin and Ullrich*, 1973; *Mège and Masson*, 1996], suggesting that in some instances graben formation should have been associated with dike emplacement [*Mège and Masson*, 1996; *Wilson and Head*, 2000; *Ernst et al.*, 2001]. Some pits have a well-preserved conical shape and display evidence of mass wasting on the floor, whereas some others have flat floor and were filled in almost entirely by smooth materials, probably lava flows fed by ring dikes during pit collapse [e.g., *Best and Christiansen*, 2001, p. 220]. Well-known terrestrial analogs include pit craters at Kilauea [*Carr and Greeley*, 1980] thought to have formed by stoping over a propagating dike [*Okubo and Martel*, 1998].

[15] Although pits and troughs are frequently observed to lie along the grabens and parallel to the border faults, in some areas pit crater chains are not associated with extensional faulting, or follow en échelon patterns oblique to grabens with an angle on the order of 15°. In areas where evidence of crosscutting relationships are found, pit craters and other depressions are always observed to cut graben border faults, which shows that they were systematically formed later. No argument has been found as to the time span between grabens and pit crater formation.

1.2.2. Elongated U-shaped Troughs, Shallow Flat-Floored Depressions, and Small Chasmata

[16] In many areas such as Valles Marineris it can be observed that a full range of transitional morphologies exist between coalescing pit chains and elongated U-shaped troughs (Figure 3c). Elongated U-shaped troughs are morphologically analog to the selenic slot-shaped vents [*Greeley and Schultz*, 1977]. Formation by collapse between individual pit craters is supported by well documented terrestrial analogs, especially at the Snake River Plain (King's Bowl) [*Greeley et al.*, 1977]; Wild Horse Corral vent [*Greeley*,
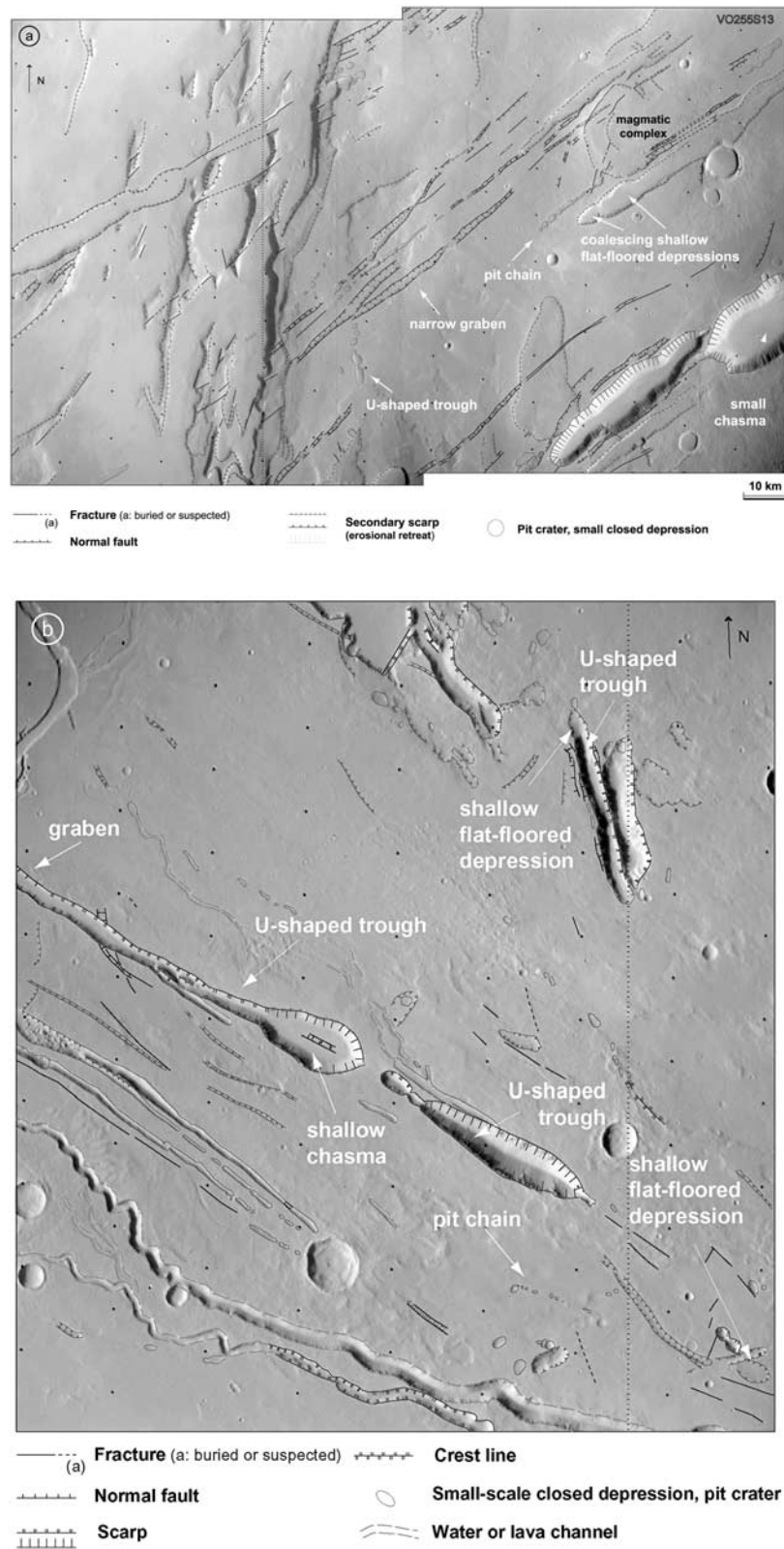
Figure 3. Depressions associated or aligned with narrow grabens at (a) Mareotis Fossae, (b) Elysium Chasma, and (c) Coprates Catena (southeast of Valles Marineris). NASA/JPL Viking Orbiter 1 images 255S11-13 (79 m/pixel), 541A37 (143 m/pixel), and 610A07 (200 m/pixel).
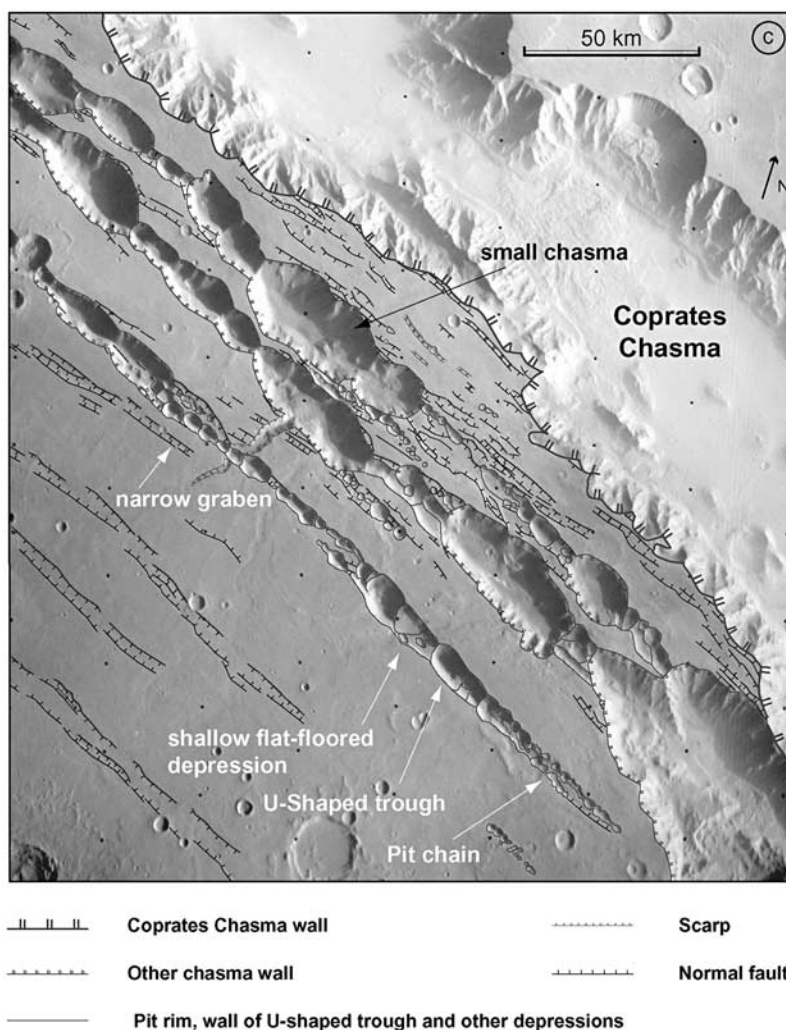
Figure 3. (continued)

1977a]; Hell's Half Acre vent [*Karlo*, 1977]; Snowdrift Crater and volcanic depressions of the Inferno Chasm [*Greeley*, 1977b] in Hawaii (Mauna Ulu summit vent, whose mechanisms of formation could be observed during the 1969–1974 eruption [*Carr and Greeley*, 1980]), and at the Erta Ale in Afar [e.g., *Tazieff*, 1973]. Shallow flat-floored depressions are interpreted as lava ponds in volcanic vents by analogy with terrestrial observations [e.g., *Greeley*, 1977b].

[17] Chasmata are of two kinds. The largest chasmata observed at Valles Marineris are mainly tectonic structures that were subsequently enlarged by mass wasting processes [e.g., *Peulvast et al.*, 2001], but the case has been made of earlier pretectonic trough initiation [*Schultz*, 1998]. Small chasmata discussed in this paper, such as on Figures 3b and 3c, display little observational evidence of faulting. We think that alignment with morphologic types of volcanic origin argues in favor of volcanic collapse origin. The difference between U-shaped troughs and chasmata may primarily be a matter of size and depth of the collapsed roof of the underlying magma body.

[18] In some regions the formation of the linear troughs, and the chasmata, has been ascribed to surface material collapse into deep tension cracks opening at a crustal level coinciding with the depth at which border faults connect [*Tanaka and Golombek*, 1989]. Following several previous works [*Schultz*, 1988; *Mège and Masson*, 1996; *Wilson and Head*, 2000; *Scott et al.*, 2000; *Mège*, 2001], we favor the volcanic hypothesis because of the apparent lack of terrestrial analogs of large linear collapse structures along tension cracks, the many terrestrial analogs described, and the markedly volcanic modified narrow graben setting. This interpretation is consistent with evidence from MOLA altimetry data that assuming constant crustal density, the alignments of narrow chasmata and catenae around the major Valles Marineris chasmata are associated with abnormally thick crust [*Zuber*, 2001]. Accounting for crustal density variations associated with linear magmatic intrusions below the pit crater chains would tend to remove the excess crustal thickness and provide a satisfactory alternative interpretation of the gravity field.

1.2.3. Linear U-shaped Troughs

[19] In some places, such as Memnonia Fossae, linear U-shaped troughs have been interpreted as collapse features resulting from dike tips approaching groundwater or ground ice level [*Mège and Masson*, 1996; *Montési*, 2001]. Frequent association with pit craters and elongated U-shaped

a pit craters (Acheron catena)
b elongated U-shaped trough (Tractus catena)
c shallow flat-floored depression (Tempe Fossae)
d linear U-shaped trough (Sirenum Fossae)
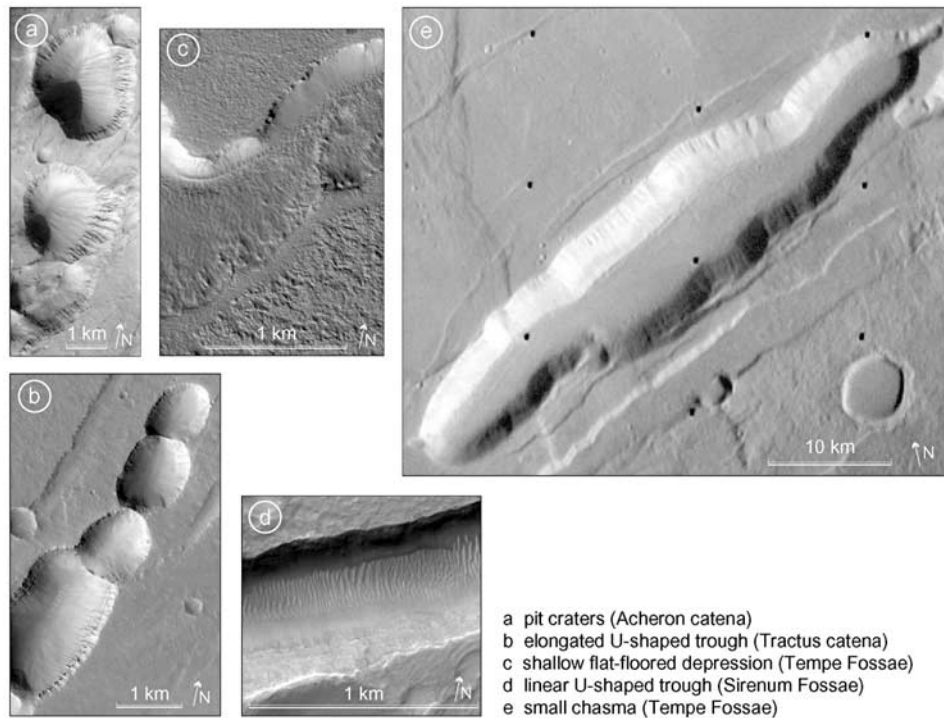e small chasma (Tempe Fossae)

Figure 4. High-resolution views of typical morphologic types discussed in this paper: (a) pit craters: Acheron Catena, part of MOC image M09-05624 centered at 107.08°W, 34.37°N, 3.05 m/pixel; (b) elongated U-shaped trough: Tractus Catena, part of MOC image M03-06623 centered at 101.26°W, 33.32°N, 3.04 m/pixel; (c) shallow flat-floored depression from Mareotis Fossae: part of MOC image M08-04991 centered at 80.01°W, 41.00°N, 3.08 m/pixel; (d) linear U-shaped trough, Sirenum Fossae: part of MOC image M17-000691 centered at 52.61°W, 31.27°S, 1.40 m/pixel; and (e) small chasma in Mareotis Fossae (medium-resolution Viking Orbiter image 255S13 centered at 84.09°W, 39.5°N, 79 m/pixel). MOC images by NASA/JPL/MSSS; Viking Orbiter image by NASA/JPL.

troughs suggests that the depressions formed by collapse above magma bodies [*Mège and Masson*, 1996; *Mège et al.*, 2000]. High-resolution (MOC) images commonly show that linear U-shaped troughs widen through landsliding and the retreat of unstable normal fault scarps (e.g., Figure 5). Linear U-shaped troughs are common in southwestern Tharsis (Memnonia, Sirenum and Icaria Fossae) and N and NE of Alba Patera. (Tantalus Fossae).

1.2.4. Graben Formation and Collapse Mechanisms

[20] On Earth, oceanic rifts at slow spreading ridges (and in places on fast spreading ridges [*Lagabrielle and Cormier*, 1999]) are examples of elongated and segmented narrow grabens thousands of km long in a volcanic setting, associated with a broad-scale stress field. They may be good structural analogs of planetary narrow grabens, even though oceanic expansion has not occurred there. This paper investigates the interaction between tectonic extension and magmatic processes with the view to proposing a comprehensive model of narrow graben, and modified graben formation, by a mechanism akin to volcanic rifting on Earth.

[21] In terrestrial volcanic rift tectonics, dikes are major connectors between deep and surface processes [e.g., *Forslund and Gudmundsson*, 1991]. It has been observed that some giant mafic dike swarms in terrestrial hotspot setting [*Ernst et al.*, 1996] are of similar length to Martian grabens [*Mège and Masson*, 1996; *Ernst et al.*, 2001]. On these grounds, geologic mapping of the relationships between grabens and volcanic landforms on Mars has led to the interpretation that the modified grabens may have formed above giant mafic dikes [*Mège and Masson*, 1996; *Wilson and Head*, 2000; *Scott et al.*, 2000] akin to the dikes in the giant terrestrial swarms. Similar interpretations have been made on the Moon [*Head and Wilson*, 1994] and Venus [*McKenzie et al.*, 1992; *Grosfils and Head*, 1994a, 1994b; *Koenig and Pollard*, 1998]. This popular tectonic concept involves a common mechanism whereby graben open at surface simultaneously to dike emplacement at depth on most silicate planets. This would occur in response to the driving pressure (ambient stress minus magma pressure) during dike emplacement. The giant swarms inferred on Mars would be either radial or concentric around major volcanic centers, which has justified comparison with those terrestrial giant dike swarms that radiate from hotspot centers [*Ernst et al.*, 1995]. The dikes from giant mafic swarms are classically considered to have flown upward above the melting source and laterally toward outer regions [*Ernst and Baragar*, 1992], although the case for vertically fed radiating swarm has been made [*Kumarapeli et al.*, 1990]. If an analogy with Martian dikes exists the dikes should probably be mafic as well in order not to cool too rapidly before freezing.

[22] However, there are several unanswered problems with the dike interpretation, such as structural relationships between individual dikes and grabens of the size observed.
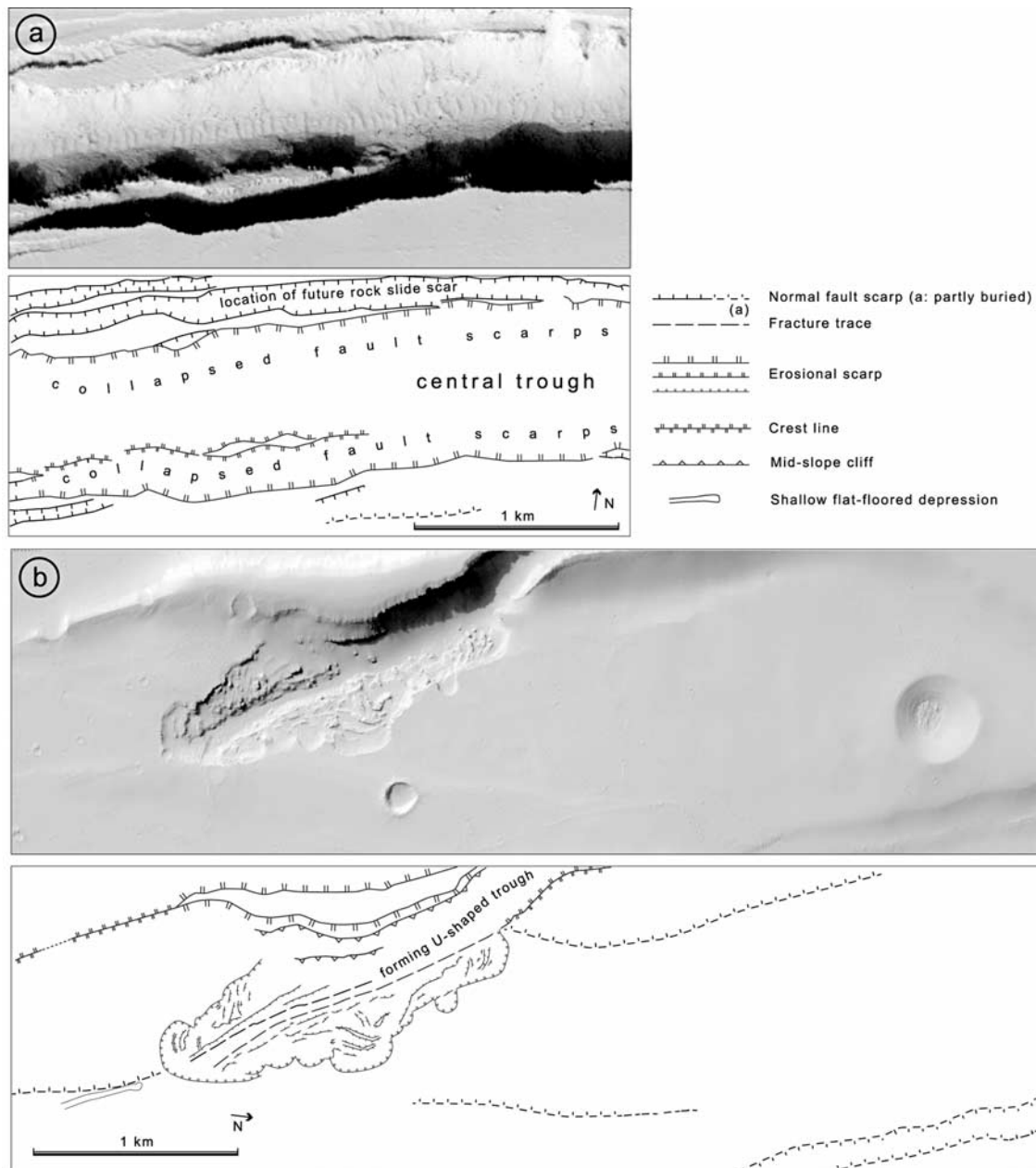
Figure 5. High-resolution image of two troughs being broadened, forming a U-shape profile from normal fault scarp destabilization and landsliding. The trough in Figure 5a fed a lava pond east of the area displayed on this image. Ceraunius Fossae, part of MOC image M09-05279 centered at 110.53°W, 28.33°N, 4.53 m/pixel. MOC image by NASA/JPL/MSSS.

On the one hand, models ascribing graben opening to driving pressure are grounded on extrapolation of simple numerical and laboratory experiments there were designed for other purposes and may not apply at the depth giant dikes are thought to propagate at high lithostatic pressure. Moreover, driving pressure cannot explain volcanic collapse, which is the key argument for the interpretation of existing magma body underlying grabens since faulting does not inform on stress source. On the other hand, models of pit and trough formation by magmatic processes have not investigated relationships with grabens nor discussed the empty volume that can reasonably be made available by magmatic collapse at the top of single dikes. Therefore, in the first step this paper thoroughly examines the arguments on which the dike emplacement interpretation has been based in order to show that in most cases dike emplacement is simply not enough to explain graben formation. Instead of tectonic stretching associated with emplacement of single dikes, this paper proposes that individual grabens displaying volcanic morphology may be akin to individual rift zones such as those observed at plate boundaries on Earth. The dikes in the rift zones are underlain by magma reservoirs elongated along graben trend. The likely absence of plate recycling on Mars (*Sleep* [1994a] presented an alternative

view) has precluded oceanic expansion from operating at modified grabens so that modified graben evolution may be compared with a short tectonic and magmatic rifting period at oceanic rifts.

[23] In a second step the relationships between magmatic processes at depth and surface processes are investigated. The collapse depressions associated with the volcanic processes that accompany rifting are measured by volume extraction from DEMs. The depth and thickness of the deflating body are determined from the geometry of grabens and troughs using experimental models. Where mass wasting has removed the initial geometry of grabens and pits, the experimental models are no longer of use, and the depth and size of the deflating magma body are investigated using three-dimensional boundary element modeling for variable magma pressures.

2. Surface Stretching and Dike Driving Pressure

2.1. Theory

[24] Terrestrial graben formation, in relation to magmatic activity, has been investigated on active volcano flanks or in a rifting setting. In these regions shallow dike emplacement was seismically correlated with the opening of graben centimeters to tens of centimeters high. Linear Elastic Fracture Mechanics (LEFM) predicts that two extensional stress peaks will be observed at the surface on both sides of a dike propagating at depth [*Pollard and Holzhausen*, 1979; *Pollard et al.*, 1983]. If the driving pressure overcomes the tensile strength of the host rock, then surface failure will occur as tension cracks [*Schultz*, 1996], a pattern that is also observed in experimental models of dike emplacement [*Mastin and Pollard*, 1988]. Experimental models of successive magma injections, within the same dike fracture, predict that the tension cracks at surface will gain a vertical offset, and gradually join deeper fractures until a graben forms [*Mastin and Pollard*, 1988]. These models provide (with some uncertainty) quantitative relations allowing one to infer dike depth from graben border fault spacing, and also dike width and from horizontal strain. The models have been used to infer subsurface dike geometry on Venus [*Grosfils and Head*, 1994b], the Moon [*Head and Wilson*, 1994], Mars [*Mège and Masson*, 1996], and at an East Pacific rise segment [*Chadwick and Embley*, 1998].

[25] However, several lines of evidence suggest that driving pressure may have only marginally contributed to planetary narrow graben formation and evolution. First, there is no need for driving pressure to form the narrow grabens. Existence of many unmodified narrow planetary grabens parallel to modified grabens (and of likely similar age) suggests that the magnitude of the ambient stress field should have been strong enough to produce narrow grabens alone. Moreover, stretching at the giant Valles Marineris graben system during a large part of the Tharsis history, (in close proximity to narrow grabens and parallel to them) clearly shows that the ambient stress was high enough to produce significant extensional strain without the help of dike driving pressure. Furthermore, observation that collapse features usually cut narrow graben structures and are associated with additional faulting suggests that if dike overpressurization is involved in graben formation, a subsequent mechanism of both extensional faulting and surface

collapse is anyway required. As normal faulting is usually involved in volcanic collapse [*Roche et al.*, 2000], faulting induced by driving pressure is unnecessary. This issue is further discussed and complemented hereafter.

2.2. Critical Assessment of Terrestrial Examples

[26] Graben formation associated with the propagation of meter-scale width dikes has been reported in Hawaii, Iceland, the Asal-Ghoubbet rift, and Etna. The observed surface strain at these sites was compared with results from LEFM and experimental models [*Pollard et al.*, 1983; *Mastin and Pollard*, 1988; *Rubin*, 1992; *Bonafede and Olivieri*, 1995]. Theoretical displacement patterns could in general match the observed geodetic displacement patterns, though the predicted displacement magnitude was not accurately reproduced in every case. Our interpretation of graben formation above the emplacing dike at the Krafla fissure swarm of Iceland, and Asal-Ghoubbet rift zone in Afar [*Pollard et al.*, 1983; *Rubin*, 1992], is that dike emplacement could instantaneously increase the deviatoric tensor, that was already near to failure, and consequently release stress gradually built at the plate boundary above the emplacing dike. This stress would have been released later anyway, although possibly elsewhere.

[27] At the Kilauea southeastern rift zone [*Pollard et al.*, 1983], where long term volcano flank landsliding is observed, magma pressure may have also added the small stress increment that triggered slope failure, whereas most of the deviatoric stress is from gravitational origin. Recurrent dike dilation pulls the volcano flank laterally, and normal faulting at surface may only result from the lateral free boundary, which results in flank gravity destabilization, as discussed by *Elsworth and Voight* [1996] and *Morgan et al.* [2000]. Moreover, between 1976 and 1982 abundant seismicity occurred despite dike emplacement quiescence [see, e.g., *Cayol et al.*, 2000] and suggests that dike intrusion may only be one of several mechanisms by which volcano flank seaward spreading occurs. Additional evidence that magma pressure has played a minor role is that if the magma pressure in shallow dikes was to play a key role in graben formation, then the southwestern rift zone should be much wider than it is actually observed [*Garcia and Davis*, 2001]. In these three cases, (Iceland, Afar, and Hawaii) the source of ambient stress is long lasting. This suggests that a large part of the stress released through graben formation would have been released anyway but later if dike emplacement did not occur. It also suggests that the key role of dike emplacement may not be graben formation, rather, at most, initial strain focus above the dike.

[28] Several lines of evidence support this view. (1) In LEFM models, the total vertical displacement modeled at surface above the dike is significantly smaller than the observed displacement [*Pollard et al.*, 1983, Figures 13 and 14], suggesting that additional remote stress played a role in the total strain measured. (2) A far better agreement between measured and modeled displacement is obtained if the graben border faults were already formed when the dike propagates. In that case the propagating dike will only induce fault slip ahead of the dike [*Rubin*, 1992]. This shows that dike emplacement can induce graben formation if a remote stress has already begun the work. (3) Experimental models predicting dike-induced grabens [*Mastin*

and Pollard, 1988] were not scaled according to mechanical scaling laws [*Hubbert*, 1937]; instead, the physical parameters of the crust were adjusted until grabens similar to those observed in nature could be reproduced. *Mastin and Pollard* [1988] have clearly warned against misinterpretations by emphasizing that their results only provide ''a possible model for deformation that can be studied by direct observation''. (4) In the Etna example, a gravity anomaly study has shown that a graben formed above a dike months after the dike was emplaced [*Bonafede and Olivieri*, 1995]. In addition, the magnitude of the observed anomaly is significantly larger than that be predicted by simple dike intrusion, suggesting that the relationships between dike emplacement and graben formation may be more complex than expected from simple models of pressurized dike emplacement.

2.3. Assessment of LEFM From Field Observations at Large Igneous Provinces

[29] Perhaps the best terrestrial analogs of the Tharsis and Elysium volcanic provinces on Mars [*Mège and Masson*, 1996; *Mège*, 2001] are dikes in large igneous provinces that are usually nonfeeders. This has been explained by dike propagation in the neutral buoyancy zone (NBZ) in the crust [*Turcotte*, 1990; *Lister and Kerr*, 1991], which on terrestrial continents has been estimated to ca. 3 km depth [*Lister and Kerr*, 1991; *Wilson and Head*, 1994]. A strong argument against major influence of driving pressure on graben formation is that high confining pressure at typical NBZ depth on Earth probably renders LEFM modeling inapplicable [*Rubin*, 1993]. More appropriate is cohesive zone dike modeling, an approach that is not designed to predict host rock behavior around dike tip but makes surface fracturing highly unlikely [*Rubin*, 1993].

[30] Field evidence at mafic dike upper tip usually confirms that cohesive zone modeling is more appropriate than LEFM. LEFM predictions may be tested two ways in the field. First, in elastic models stress concentrate at dike tip, where theoretically stress becomes infinite [e.g., *Pollard et al.*, 1983], so that although LEFM does not allow that dike stops propagating. If for some (unpredicted) reason this occurs, one would expect the dike tip profile at a given segment to be linear or penny-shaped, a feature that can be readily tested in the field. Second, a graben should form above the dike, which is also easily tested in the field in areas where erosion allows. Surface strain should scale with magma overpressure, which also partly governs the width of the dike during the intruding event, in conjunction with other factors [*Rubin*, 1993].

[31] Observations at large igneous provinces do not confirm either of these predictions. Analysis of magma flow in meter-wide mafic dikes as well as field observation of internal chilled margins in thicker dikes suggest that if wall meltback does not occur (in which case dike growth does not affect the stress regime [see *Bruce and Huppert*, 1990; *Fialko and Rubin*, 1999]), most mafic dikes thicker than ca. 1 m were formed by more than 1 magma injection [*Gudmundsson*, 1984; *Baer*, 1995; *Platten*, 2000]. In Iceland, the dike width near upper tip is commonly 0.5–2 m, which probably reflects dike dilation during the last injection event [*Gudmundsson*, 1995a]. Therefore emplacement of thick dikes, such as those required for explaining narrow graben formation by driving pressure, are achieved through

many magma pulses. This has major implications in terms of strain distribution. In order for a magma pulse to inject into an earlier dike fracture, the magma previously intruded should not be fully solidified. Magma emplacement during a given magma pulse is frequently associated with tensile fracturing parallel to the dike plane on both sides of the dike upper tip [e.g., *Delaney et al.*, 1986]. These fractures are filled in by subsequent injected magma, which allows the new sheet to attain a shallower level in the crust and create new small-scale fractures above the new tip [*Gudmundsson*, 1995a]. Every new magma injection fills in the fractures formed by the previous injection above the propagating dike tip. This results in the common observation that even the thickest vertical dikes gradually narrow upward toward the upper tip zone, where they suddenly display a one to tens of meter-scale sawtooth/sickle geometry in vertical cross section (e.g., *Gudmundsson* [1984, 1995a] and personal observation by the authors in various regions). As a result, country rock fracturing resulting from the whole dike injection history does not take the form of broad-scale tectonic structures. After the last injection, fracturing at dike tip is never larger than what would have been expected from a single intrusion event. Therefore, even though 10 to 100 meter wide dikes (resulting from multiple injections) attain a crustal depth that is shallower than the depth of a single dike injection, surface fracturing above the dike is negligible. Moreover, field observations at mafic dikes, including dikes tens of meters thick, frequently shows that the uppermost dike tip segment is tapered, or snakes within the host rock over distances of centimeters to a few meters. Frequently the dike tip follows existing rock discontinuities [*Gudmundsson*, 1984; *Delaney et al.*, 1986], or grain boundaries [*Hoek*, 1994, 1995]. These observations suggest low pressure at the dike tip, and favor cohesive zone models of dike tip rather than LEFM. Finally examination by the authors of terrains located above dike tips, in various igneous environments, for example, the Ethiopian igneous province, never revealed examples of grabens located directly above the tip. This is confirmed by observations reported in the literature [e.g., *Gudmundsson*, 1984]. Possible examples of grabens located above dike tips would be interpreted as evidence that both may have formed in a similar or the same stress field, for instance a regional mantle plume-related extensional stress field. It would not provide any evidence as to the role of magma pressure in graben formation.

2.4. Extrapolation to Planetary Narrow Grabens

[32] Terrestrial observation above narrow and shallow dikes (ca. 1 m) shows that the location of graben border faults may be influenced by dike emplacement location in certain circumstances, but the study of large igneous provinces argues against extrapolation to large dikes. Extrapolation to planetary narrow grabens needs in addition to consider the difference in gravity between the Earth and Mars. Planetary narrow grabens (as defined from Viking imagery) are typically 2–5 km wide and a few hundred meters deep. In order for graben formation to have been influenced by driving pressure the dikes would need to be much wider, ($\sim$30–1000 m) and deeper (0.3–2 km) than in the above terrestrial examples, in order to match graben width and observed fault offset [*Mège and Masson*, 1996]. Most dikes would need to be hundreds of meters wide. This width must

be produced without the help of dike wall meltback, which increases dike thickness without generating additional stress and is therefore of no help in graben formation.

[33] If wall meltback is not accounted for, the maximum width of planetary mafic dikes associated with planetary grabens can be independently estimated for every planet using mechanical laws such as those summarized by *Wilson and Head* [2000] using a range of plausible mechanical parameters. For Mars, *Wilson and Head* [2000] found that the thickness of dikes propagating at the NBZ can hardly exceed 100 m. However, according to the experimental models by *Mastin and Pollard* [1988] such dikes are still significantly too narrow to play a major role in the observed border fault throws. Moreover, maximum dike width is also controlled by the tensile strength of the host rock. The largest crustal earthquakes on Earth may give clues as to the maximum tensile stress a silicate crust can support before it fails, i.e., to the maximum stretching that can be instantaneously produced. Horizontal displacement produced by large earthquakes on Earth at great crustal depth is on the order of less than 10 m, which should provide an upper bound of maximum instantaneous dike dilation (the real value should actually be smaller because the largest earthquakes are in compression and rocks are weaker in tension). Therefore, even though maximum thickness attainable by a dike propagating at the Martian NBZ is predicted to be greater than on Earth, host rock strength does probably not allow this thickness to be reached. Thick dikes should either be emplaced by a succession of many injections, or from the thermal erosion of dike walls, resulting in a low available stress for graben formation in both cases.

[34] On Venus, where the NBZ is thought to lie at 1.4 km below the surface and may not even be present at lower elevations [*Head and Wilson*, 1992; *Wilson and Head*, 1994], *Koenig and Pollard* [1998] showed that dike injection alone cannot provide enough stress to form narrow grabens, and suggested that regional tectonic stress such as provided by rifting and gravitational spreading must have been important factors in graben development. Under Martian conditions, for NBZ propagating dikes the combination of low atmospheric pressure and low gravity (compared to terrestrial conditions) both contribute to a dramatic NBZ depth increase to 10–11 km for mafic magmas, depending on magma CO_2 content [*Wilson and Head*, 1994]. The likelihood for such dikes to generate enough stress to form narrow grabens is therefore weak. The same conclusion arises from the basic reasoning that if magma pressure was to play a major role in graben formation, it would necessarily generate contractional structures parallel to the grabens in order to compensate for the sudden localized stretching. We conclude that driving pressure may only occasionally induce graben formation.

3. Surface Stretching and Central Collapse by Pressure Drop

3.1. Pressure Drop

[35] Pressure drop occurs if part of the space the magma body has occupied is emptied because of magma migration or compaction, and requires that the rate of magma supply be lower than the deflation rate, or null. Eruption is an efficient way for magma removal from subsurface that causes caldera subsidence by pressure drop. In an extensional setting, rift propagation also results in magma migration, which may in turn result in surface collapse. More rapidly, lateral magma flow in a dike fracture may induce stoping in the country rock above the dike and surface collapse [*Okubo and Martel*, 1998]. Host rock fracturing because of gas overpressure above the magma body [*Liu and Wilson*, 1998], and removal of interstitial melt [*Lagabrielle and Cormier*, 1999] are other processes that may also induce surface collapse.

[36] Models of collapse trough infrastructure have been recently reviewed [*Burov and Guillou-Frottier*, 1999; *Roche et al.*, 2000]. The role of several important factors has been recently investigated, such as reservoir roof aspect ratio [*Roche et al.*, 2000, 2001] and thermal effects of hot magma [*Burov and Guillou-Frottier*, 1999]. Mechanisms of pit crater formation has been specifically addressed by *Roche et al.* [2001], who found that two mechanisms, slow rigid block subsidence or rapid stoping, may be involved depending on roof aspect ratio. Subsidence would occur for roof thickness smaller than roof diameter, whereas stoping would be favored in other cases. In both collapse types, reverse faults play a major role in collapse even though surface deformation always ends up with extensional structures, because of gravitational instability of reverse faults at the surface. In order to understand relations between magma deflation and stretching at volcanic rifts following an experimental procedure *Lagabrielle et al.* [2001] and *Garel et al.* [2002] have investigated the case for collapse along linear trends - this is similar to that reported in the present work.

[37] Pressure drop may be accompanied by normal faulting aligned with the direction of the deflating body. Deflation may thus induce graben formation even though the remote stress magnitude is null [*Lagabrielle et al.*, 2001]. Before going into more detail we discuss the size of collapse features and infer the type of required magma body.

3.2. Type of Magma Body and Volume of Deflated Materials

3.2.1. Dike or Magma Reservoir?

[38] Available topography data and images show that the width and depth of most observed collapse features on Mars are in the range $10-10^4$ m and $10-10^3$ m, respectively. Therefore only the smallest collapse features may be associated with pressure drop above single dikes. An example of pit craters associated with single dikes is given on Figure 6a. The dikes follow the Acheron and Tractus catenae NE-SW trend and have probably the same origin. Most pit craters observed at medium (Viking) resolution, i.e., most of those studied in this paper and earlier papers, are much larger and suggest larger magma bodies. Figure 6b shows an example where it is unlikely that pits and elongated U-shaped troughs formed by pressure drop along a single dike (even a segmented dike), because their distribution does not follow several linear trends with no en échelon geometry. If the collapse features in this example are to be aligned along linear trend, then several subparallel dikes are required, suggesting that the models predicting formation of a single graben from driving pressure during the emplacement of single dikes are not appropriate. An alternative hypothesis is that collapse occurred above an elongated reservoir aligned with the graben trend. Alignment of
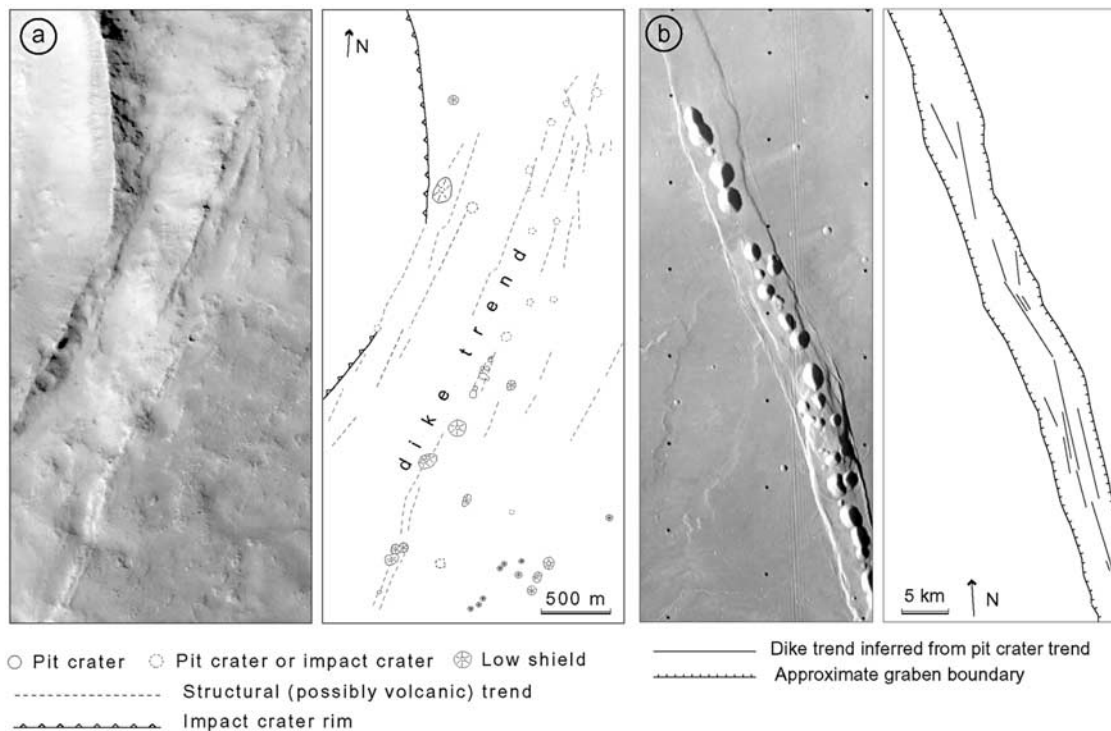
Figure 6. (a) Pit craters associated with single dikes near Tractus Catena. The pit craters have width <100 m, which is comparable to the small pit craters in Hawaii [*Okubo and Martel*, 1998]. Part of MOC image M16-00592 centered at 105.66°W, 34.25°N, 4.57 m/pixel by NASA/JPL/MSSS. (b) Dike trends inferred from pit crater alignment within Tractus Catena graben, assuming that every pit crater is located above a single dike. A single segmented dike cannot explain the distribution of all the pit craters. Either a series of aligned dikes or a broader magma body is required. Part of NASA/JPL Viking Orbiter image 252S20 centered at 118.6°W, 36.44°N, 75 m/pixel.

pits and elongated U-shaped troughs with small chasmata (Figure 3) favors the interpretation that such elongated reservoirs do exist. In volcanic rift zones on Earth, magma reservoirs usually underlie and feed parallel dikes (see below), so that both a reservoir and overlying dikes would exist below the Martian grabens. In order to discuss the magmatic infrastructure issue further, we calculate the volume of collapse troughs from topography data to constrain the volume of removed materials, which may approximate the volume of erupted materials.

3.2.2. Volume of Removed Materials

[39] Trough volume is extracted from the DEMs using a method that fills in the trough, starting by the lower digital number (DN) value (at the bottom of the trough) and gradually filling the depression upward until the desired DN value, which is the value of the plain or plateau elevation that surrounds the trough. The method, detailed in the appendix, uses MOLA data and in areas where Viking stereoscopic coverage exists and is appropriate, combination of MOLA data and stereoscopic imagery (Figure 7).

[40] Many troughs are large enough for their volume to be measured with the available data. Most individual pit craters, however, and the smallest central troughs are too small. We measured volumes of various trough types at Tractus Catena, Mareotis Fossae and the Valles Marineris area (Figures 7 and 8, Table 1). The volumes are between 14 and 420 km³. To compare with a terrestrial volcanic province, this range is at the lower end of the volume of

the individual lava flows that make the Columbia River flood lavas. The volume of the individual lava flows in the Grande Ronde basalts, which make most of the Columbia River basalts, is between 90 and 2500 km³ [*Reidel et al.*, 1989]. By comparison with the Columbia River basalt eruptions, the collapse features along the structural trends may be fed by individual dikes that channeled magma from a deeper reservoir to the surface. Then magma withdrawal from the reservoir would have induced surface collapse. The volume of removed material during every collapse event at modified grabens, or at depressions aligned along a structural trend such as some catenae and many chasmata, may have formed by a single eruption event contributing to volcanic construction of the major Martian volcanic shields. The volume of individual pit craters, which could not be measured, could in some cases result from collapse above single dikes, as on Figure 6a, from comparison with terrestrial pit craters having size only slightly smaller than those observed on Mars [*Okubo and Martel*, 1998].

4. A Qualitative Model of Volcanic Rifting on Mars

[41] Channeling the magma from a reservoir to the surface requires that dikes were injected from the reservoir, so that both a reservoir and subparallel dikes should lie below the grabens. Modified narrow grabens may thus be akin to terrestrial volcanic rift segments. Analogy with volcanic

Figure 7. Digital elevation model of part of Mareotis Fossae. The whole area is covered by the MOLA digital elevation model. The lighter part of the DEM emphasizes the area where Viking stereo coverage (used image numbers shown) has improved the resolution of the MOLA digital elevation model. For this area, DN height resolution is 15 m.

rifts at terrestrial plate boundaries is further illustrated with the East Pacific Rise, Iceland, and Asal-Ghoubbet rifts.

4.1. Comparison With Morphology of the East Pacific Rise

[42] Noting that the narrow grabens have width (2–5 km) and length/width ratio (on the order of $\sim 10^2$) similar to those at terrestrial oceanic rifts (e.g., 10 km at Icelandic rift zones, 1–2 km at the East Pacific Rise), we suggest that morphologic evolution at Martian narrow grabens and at terrestrial oceanic rift zones present similarities that reflect several common structural and magmatic processes even though the geological context is different [*Mège et al.*, 2000]. Figure 9 provides examples of geomorphologic
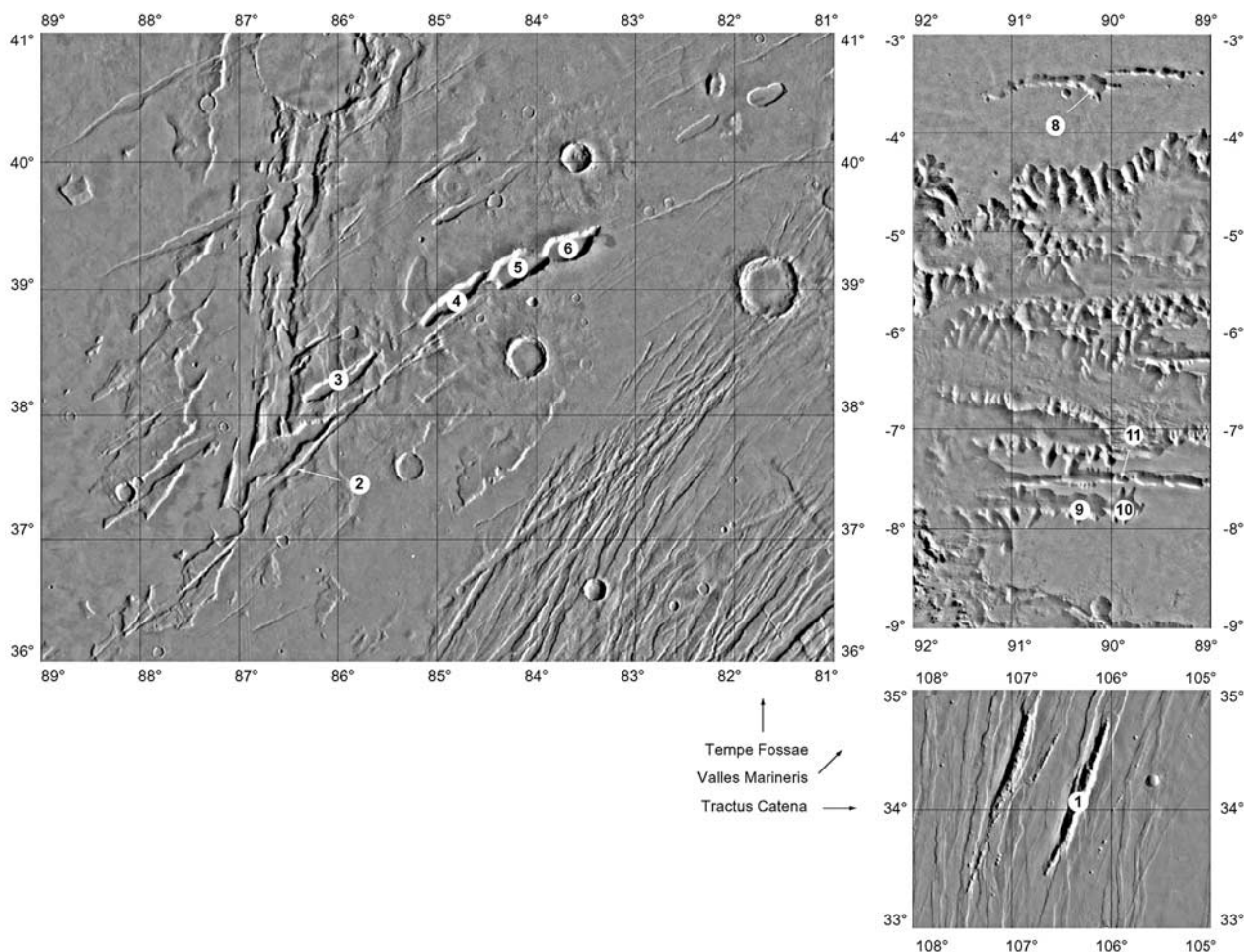

Figure 8. Location of the troughs whose volume was measured (Table 2) and compared with boundary element modeling of magma deflation (Table 3). Base maps: USGS/PDS MDIM, 256 pixels/degree, pdsmaps.wr.usgs.gov.

Table 1. Viking Orbiter Images Used in DEM Generation

	Area	Morphologic Type	Latitude, °N	Longitude, °W	Max Length, km	Max Width, km	Depth, m	Volume, km³
1	Alba Patera	catena (Tractus)	34.1	106.3	75	9	1600	420
2	Mareotis Fossae	small ovoid chasma	37.6	86.3	9	5	80	14
3	Mareotis Fossae	narrow chasma	38.3	86	45	9	280	37
4	Mareotis Fossae	narrow chasma	38.9	84.6	50	11	530	130
5	Mareotis Fossae	narrow chasma	39.2	84.2	35	14	1380	348
6	Mareotis Fossae	narrow chasma	39.3	83.7	35	14	1060	232
7	Mareotis Fossae	shallow ovoid trough	40.5	81.7	24	10	250	42
8	Valles Marineris (N Tithonium chasma)	small chasma	−3.5	90.2	13	11	560	44
9	SW Valles Marineris	small chasma	−7.8	90.2	22	14	1850	324
10	SW Valles Marineris	small chasma	−7.8	89.8	20	15	1700	265
11	SW Valles Marineris	very small chasma	−7.6	89.8	9	5	660	37

features at the East Pacific Rise that are similar to modified narrow graben features.

[43] Similar to Martian grabens, a large trough (0.5–2 km wide) notches the axial high along 15–20% of the East Pacific Rise (EPR) [*Lagabrielle and Cormier*, 1999]. Notched segments are correlated with ''robust'' magma supply (production and delivery), as characterized by a broad axial cross section and the presence of an axial magma chamber (AMC) only 1–2 km deep [*Macdonald and Fox*, 1988; *Scheirer and Macdonald*, 1993]. An overall correlation between the AMC depth and the trough dimensions as well as structural considerations suggest a volcanic rather than tectonic origin for this feature [*Lagabrielle and Cormier*, 1999]. Large axial troughs are interpreted as linear elongated collapse calderas that form when the EPR magma reservoir deforms and compacts during periods of waning magma supply [*Lonsdale*, 1977; *Kappel and Ryan*, 1986; *Macdonald and Fox*, 1988; *Lagabrielle and Cormier*, 1999; *Lagabrielle et al.*, 2001; *Garel et al.*, 2002]. This mechanism is amplified by continuous regional extension related to plate divergence, which also leads to subsidence of the top of AMC by stretching of the crystal mush [*Boudier and Nicolas*, 1996; *Dilek et al.*, 1998; *Lagabrielle and Cormier*, 1999; *Lagabrielle et al.*, 2001; *Garel et al.*, 2002]. Very high-resolution topography data also reveal the existence of aligned small constructional mounds within the axial trough (Figure 9b) [*Shah et al.*, 2003; *Sinton et al.*, 2002]. Collapsed lava lakes as narrow as 10–20 m wide are also frequently observed at the axis of accretion.

4.2. Comparison With Icelandic Fissure Swarms

[44] Rifting in Iceland occurs as en échelon grabens associated with fissure swarms. Regional dikes following the graben trend are fed by magma reservoirs rooted at a continuous magma layer at ∼10 km depth. The magma reservoir also feeds magma chambers located at 2 km depth that in turn feed volcanoes and local sheet swarms [*Gudmundsson*, 1990a, 1995b]. Field work and geophysical data allowed *Angelier et al.* [1997] and *Dauteuil et al.* [2001] to infer that most expansion at the surface occurs by tectonic stretching along tension fractures. At deep crustal levels oceanic expansion is achieved through magma dilation of the regional dikes, and at intermediate crustal level by a combination of dike dilation and normal shear fractures formed by downward propagation of tension fractures [*Gudmundsson*, 1992]. Figure 10 shows an aerial view of the Krafla fissure swarm, a typical rift zone graben in Iceland, and an interpretation sketch of the volcanic-tectonic

infrastructure of the Icelandic rift zones. This model [*Gudmundsson*, 1995b] provides relationships between tectonic structures and magmatic plumbing that are consistent with observations at modified narrow grabens on Mars as from the examples described in the present paper.

4.3. Comparison With the Asal Rift in Afar

[45] The Asal-Ghoubbet rift in Afar is another volcanic rift zone that may help understand the rifting process on Mars. Structural interpretation of the Asal-Ghoubbet rift from Spot P imagery and offshore DEM (Figure 11a) reveals striking analogy with the Tempe Fossae (Figures 11b and 11c). In both examples shown, strain has concentrated around a central volcanic edifice located within the graben (Figure 11e), which is a classical pattern predicted by stress models of overpressurized magma body in extensional setting [e.g., *McKenzie et al.*, 1992]. Similar geometry (Figure 11d) has been observed at the slow spreading North Atlantic mid-ocean ridge [*Durand et al.*, 1995]. The Asal-Ghoubbet rift results from the propagation of the slow spreading Aden oceanic rift on land [*Manighetti et al.*, 1998]; therefore both the Afar and Atlantic examples suggest that the rheology of the crust at low spreading ridges may be appropriate to the development of the Tempe Fossae rift geometry. Further comparison between rift propagation from the Aden ridge to Afar and rift propagation at Tempe Fossae on Mars is a promising topic that shall be investigated in a forthcoming paper.

[46] Fissure eruptions within the Asal-Ghoubbet rift occur along graben parallel dikes [*Le Dain et al.*, 1979] and are aligned with central volcanic edifices. Detailed analysis of relationships between tectonic structures and magmatic plumbing is underway [*Doubre et al.*, 2001] and should help assessing comparison with models of Icelandic rift zones.

4.4. Qualitative Model of Volcanic Rifting on Mars

[47] The volcanic rift examples above help understanding the relationships between surface tectonics and magmatic plumbing at Martian modified grabens. The terrestrial models are incorporated into the Martian context to propose a qualitative model of Martian rift structure. This model will then be quantified using high-resolution DEMs and mechanical models.

[48] Surface stretching started very early in the Martian history and may even predate initiation of the Tharsis volcanic province [*Scott and Tanaka*, 1986; *Phillips et al.*, 2001]. There is very little evidence of alignment of major
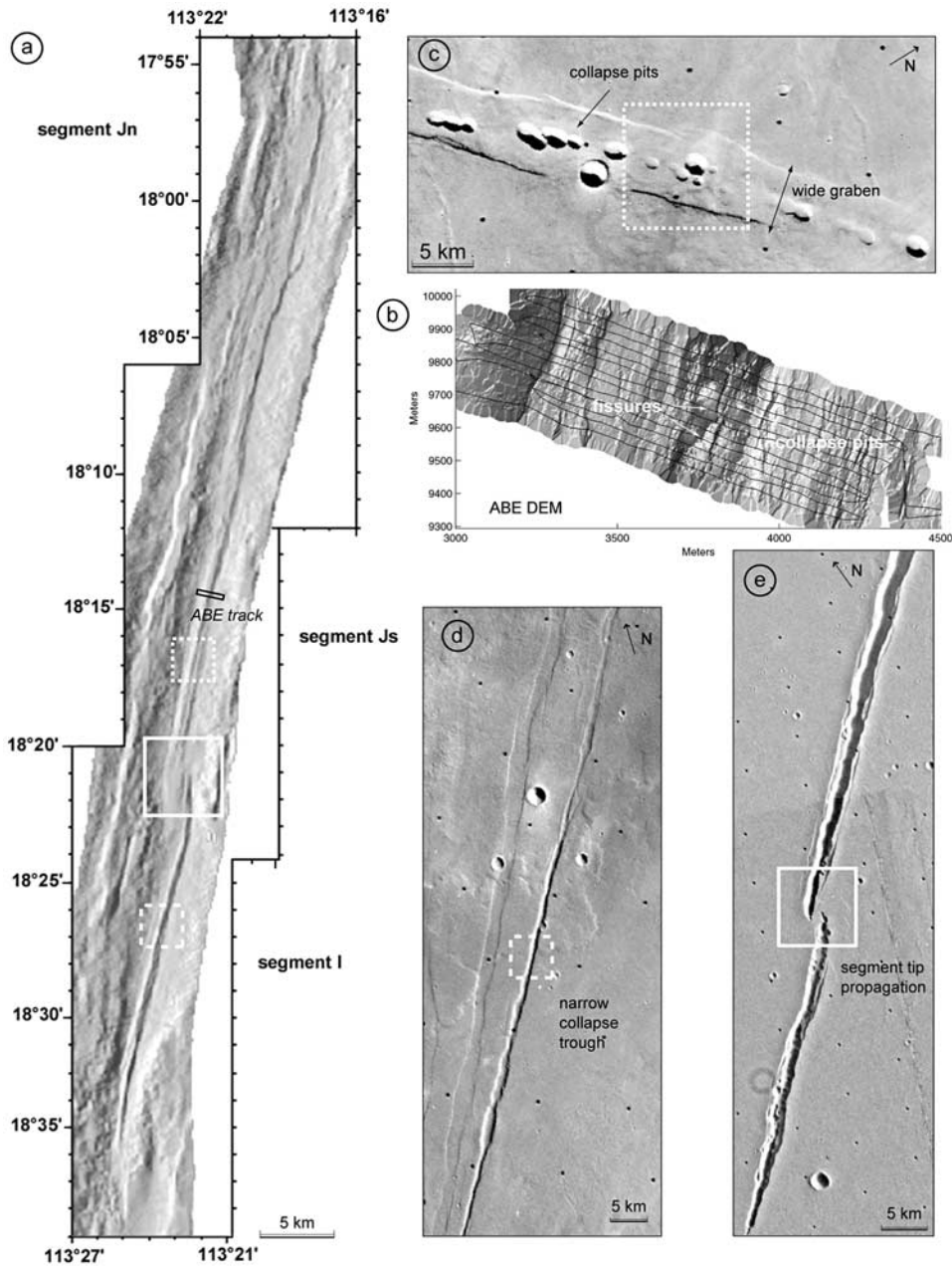
Figure 9. Analogy between morphology of segments I, Jn, and Js of the East Pacific Rise and graben morphology on Mars. (a) Digital elevation model of the East Pacific Rise. (b) Autonomous Benthic Explorer (ABE) digital elevation model along a portion of ridge segment Js (footprint 5 m), and ABE tracklines [*Yoerger et al.*, 2000; *Shah et al.*, 2003]. (c) Portion of a graben displaying a pit chain, Alba Fossae. Viking Orbiter image 252S18 centered at 118.49°W, 37.71°N, 74 m/pixel. (d) Linear trough at Tractus Catena. Viking Orbiter image 254S49, 98.05°W, 35.67°N, 66 m/pixel. (e) Linear trough at Labeatis Fossae displaying evidence of fracture propagation. Viking Orbiter images 229A32 (94.34°W, 22.33°N) and 229A34 (93.56°W, 22.61°N), 50 m/pixel. The boxes emphasize type areas displaying strong interplanetary similarity.

volcanic features (such as collapse pits, spatter ridges etc.) with grabens from this period (smaller-scale volcanic edifices are however observed at the Noachian Thaumasia grabens; Figure 2b), consequently there is no evidence for significant interaction between magmatic and tectonic activity [*Mège and Masson*, 1996]. Volcanic features are observed to be associated with grabens of Hesperian and Amazonian age, and are probably of the age of the lava flows identified in the Tharsis and Elysium regions [*Scott and Tanaka*, 1986; *Greeley and Guest*, 1987]. This suggests that both extension and large-scale thermal anomalies in the mantle were involved in the generated magmas when the grabens formed. Evidence of gigantic magma volumes is provided by: (1) the large range of Martian lithosphere
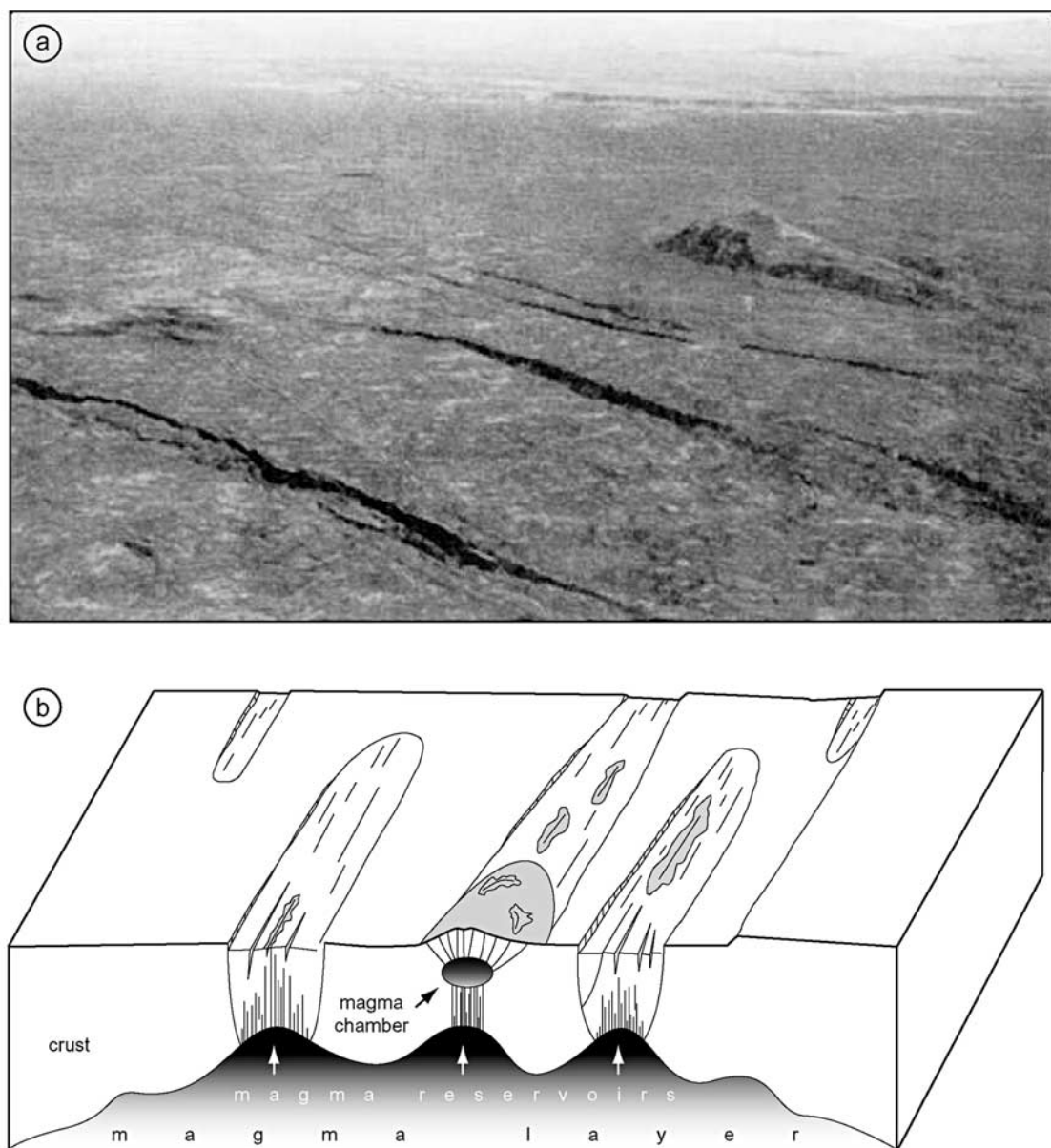
Figure 10. (a) Aerial view of the Krafla fissure swarm in Iceland [after *Opheim and Gudmundsson*, 1989] and (b) relationships between magma reservoirs, magma chambers, regional dike swarms, local sheet swarms, and surface fractures at typical Icelandic fissure swarms. Redrawn after *Gudmundsson* [1995b].

thickness that allows voluminous partial melting by mantle decompression during extension, and consequently the very high partial melting induced by any thermal anomaly, (2) the unforeseen thickness of lava flows observed over the whole 2–10 km high Valles Marineris slopes [*McEwen et al.*, 1999], which may give an idea of the thickness of the lava flows that spread over the whole Tharsis, (3) the 60–80 km thick crust in the Tharsis region [*Zuber et al.*, 2000], which emphasizes the efficiency of underplating and crustal thickening by intracrustal magma accretion.

[49] Because the crust was undergoing extension simultaneous to magmatic activity, part of the generated magma was trapped in regions of concomitant lithospheric stretching. Whether part of this magma was channeled from the

area of maximum thermal anomaly depends mainly on lithosphere thickness [*Mège and Masson*, 1996; *Kiefer*, 2000; *Mège*, 2001]. It is possible that the magma flowed laterally from the central volcanic areas (Syria Planum, Tharsis Montes, Alba Patera, Elysium Mons) to the forming narrow grabens. The mechanism involved would be analogous to magma channeling, from the hotspot center to rifts in the hotspot periphery, advocated at the Yellowstone/Columbia Plateau [*Thompson and Gibson*, 1991] and Afar/Tertiary frican rift systems [*Ebinger and Sleep*, 1998]. The magmas would have been channeled and stocked below the grabens in magma chambers whose later deflation would have induced surface collapse. Alternatively, magmas may have been mainly generated underneath
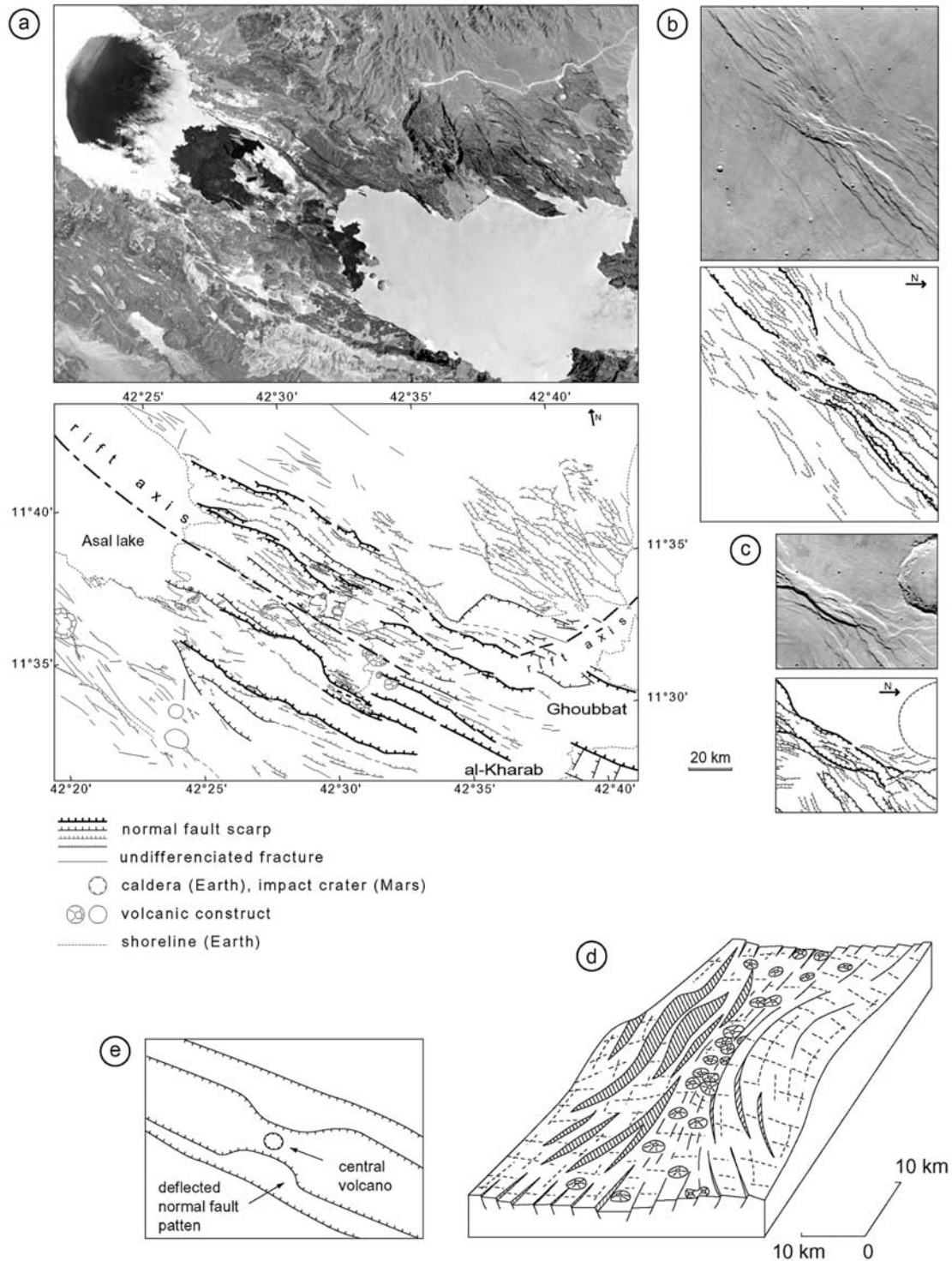
Figure 11. (a) Comparison between the Asal-Ghoubbet volcanic rift, Afar, from Spot P imagery of the Asal rift and a digital elevation model of the Ghoubbet basin from the data obtained during the Tadjouraden cruise [*Audin et al.*, 2001]; (b) and (c) part of the Tempe Fossae, Mars; (d) a segment of the North Atlantic mid-ocean ridge; and (e) summary of the basic common features. Spot P image KJ 144-327, 10 m/pixel, and parts of NASA/JPL Viking orbiter image 704B54 centered at 71.98°W, 38.05°N, 213 m/pixel.

the grabens and migrated upward to feed the magma chambers. In both cases, surface eruptions would have resulted from dikes propagating dominantly vertically from the chambers to the surface or subsurface.

[50] While tectonic stretching at surface was taking place, elongated magma chambers gradually emplaced at a deeper level (Figure 12a). The chambers may be discontinuous along strike, reflecting observation that collapse features on
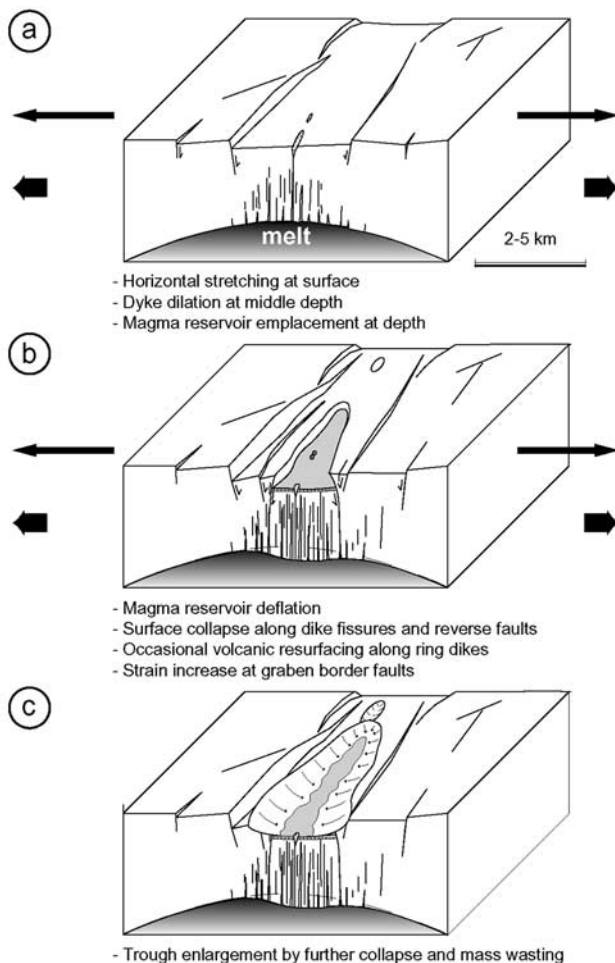
Figure 12. Qualitative sequence of magmatic-tectonic development at Martian modified grabens.

Mars are frequently observed as clusters separated by unaffected graben segments, and sometimes as en échelon segments. This is similar to terrestrial rift zones, in which magma reservoir injects dikes both toward the surface and laterally. There is no specific constraint on dike width in this model. Dike emplacement would have channeled magmatic fluids to upper levels, including the surface, inducing a gradual pressure drop in the upper part of the reservoir and eventually surface collapse (Figure 12b). Collapse may have occurred along the dike fissures. Locally, dike propagation into volatile-rich level may have induced hydrovolcanic explosions and hydrothermal flows, whose repercussions at the surface may have induced a number of small-scale volcanic landforms, as discussed by *Mège and Masson* [1996] and following mechanisms investigated by *Delaney* [1982], *Rubin* [1993], and *Bonafede and Olivieri* [1995].

[51] Many grabens display evidence of dramatic post-faulting mass wasting that removed the border fault scarps (Figure 4d). This feature appears to be common to many settings on Mars. The most spectacular evidence of large-scale postfaulting mass wasting is observed in the Valles graben system, where the period of major tectonic activity was followed by intense landsliding of the walls and the removal of fault scarps. The observations are consistent

with a period late in the geologic history of Mars where subsurface rocks lost part of their cohesion, favoring desta-bilization of the steepest slopes, maybe in relation to permafrost sublimation [e.g., *Peulvast et al.*, 2001]. What-ever the origin of late stage mass wasting at the modified narrow grabens, mass wasting resulted in volume redistri-bution. In areas where the floor is flat and smooth (seen in ~10 m resolution images), the late stage collapse event may have been accompanied by volcanic resurfacing following ring dikes. An illustration of possible modified graben subsurface structure that underwent late stage mass wasting is given on Figure 13.

[52] Apart from the troughs that underwent late stage mass wasting, it is possible to retrieve the depth of the top of the deflating magma body, and its width, from experimental models. Below we investigate these parameters under various conditions of remote stress and crustal rheology. Then numerical modeling of reservoir deflation will be performed in order to determine physical parameters that are consistent with the volumes of collapsed materials at surface.

5. Magma Deflation: Experimental and Numerical Simulations

5.1. Experimental Modeling of Graben and Trough Evolution

5.1.1. Apparatus

[53] *Garel* [1998], *Lagabrielle et al.* [2001], and *Garel et al.* [2002] carried out small-scaled experimental modeling of magma chamber deflation, in brittle and brittle ductile layers, some of them combined with horizontal extension. These experiments could provide useful insights into the development of surface features during magma deflation as well as the depth of the deflating body. The scale, fixed at 1:20,000, was based on the equality between no-dimen-sional values of the model and of the natural prototype [*Hubbert*, 1937]. The experimental apparatus used in the present study includes an inflatable elongated balloon filled with water and set in a central groove in a table as an analogue of the magma reservoir (including magma lens and crystal mush) (Figure 14). Balloon deflation is con-trolled through a pipe closed by a tap. In some experiments the balloon is capped with a silicone layer of thickness Eb representing hot rocks below the ductile/brittle transition (DBT), and is covered by a sand layer of thickness Ed accounting for the upper brittle crust. In other experiments the ductile layer is absent. Experiments integrate either or both balloon withdrawal and extension at the lateral boun-dary of the model by means of two mobile walls.

5.1.2. Withdrawal, No Applied Horizontal Traction

[54] Significant balloon deflation, without extension in a wholly brittle layer, results in the formation of a central collapse trough limited by reverse faults that are embedded within a wider graben (Figure 15, AB). In surface view, the trough trace follows the shape of the balloon at depth. Cross sections reveal that the faults are rooted at the edges of the deflating area. Experiments conducted at various balloon diameters show that reservoir depth is proportional to graben width whereas it is inversely proportional to collapse trough width (Figure 16). Similar results have been obtained in other experiments carried out by *Roche et al.* [2000].
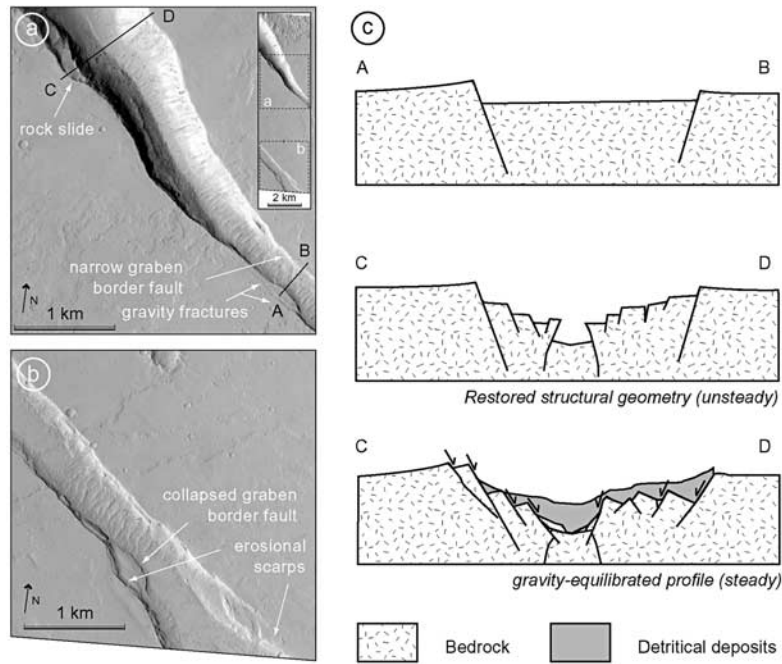
Figure 13. Possible structure and evolution of modified narrow grabens from interpretation of experimental results. (a) and (b) High-resolution image of narrow grabens changing to U-shaped trough. Part of MOC image M03-06659, 126.54°W, 9.66°N, 2.92 m/pixel. (c) Schematic morphostructural interpretation. MOC image by NASA/JPL/MSSS.

[55] The presence of a ductile layer at depth induces widening of the deformed area in response to silicone flowing toward the withdrawing zone at depth. With a ductile layer that is thick enough, ductile flow induces formation of two conjugate grabens flanking the central collapse (Figure 15, CD) instead of a single central graben.

5.1.3. Applied Horizontal Traction, No Withdrawal

[56] When extension is applied to a model having a thin or absent silicone layer, two lateral grabens develop symmetrically on both sides of a central horst (Figure 17, CD). If the ductile layer thickens, deformation distribution increases and the overall structure is more akin to a complex single graben (Figure 17, AB). Thus lateral graben formation is impeded by existence of ductile layer in case of applied horizontal traction alone, whereas it is promoted if withdrawal occurs alone.

5.1.4. Withdrawal and Horizontal Traction

[57] In brittle ductile experiments in which slight withdrawal occurs concurrently with extension, withdrawal imposes the geometry of deformation, and formation of lateral grabens is favored (Figure 18). Lateral grabens continue forming with increasing withdrawal, which ultimately ends with development of a central collapse trough in a way similar to that in experiments solely involving balloon deflation.

[58] Formation of fractures initiated in extension does not inhibit subsequent development of the collapse structures if balloon deflation occurs. Conversely, when withdrawal is
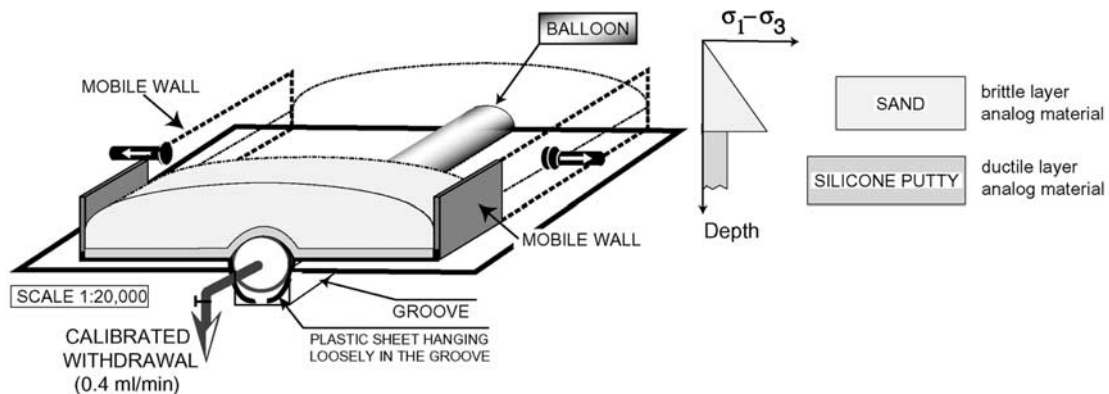

Figure 14. Experimental apparatus and the depth-strength profiles used.
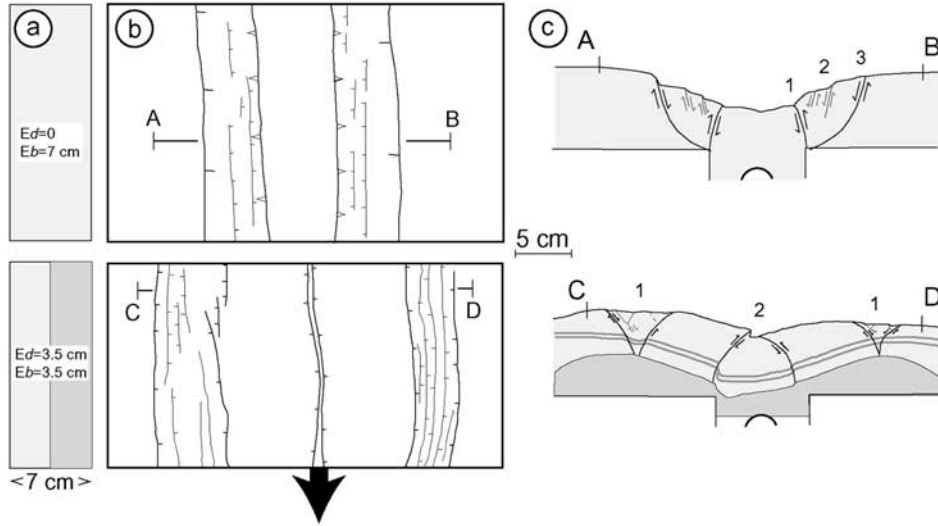
Figure 15. Results of scaled deflation experiments in brittle (Mohr-Coulomb) and brittle ductile (Mohr-Coulomb-Newtonian viscous) materials with no horizontal traction: (a) rheologic cross section (bottom to the right), E*b*, brittle layer thickness and E*d*, ductile layer thickness; (b) surface view at the end of the experiment and location of cross sections; and (c) cross sections at the end of the experiment. Kinematics and sequence of fault development are indicated.

followed by extension, the collapse structures widen in response to outward migration of the deformation wave.

5.1.5. Graben Width and Central Trough Width Versus Magma Chamber Width and Depth

[59] The experimental results provide elements for estimating magma body width and depth from surface observations, which is helpful for planetary bodies where subsurface data are unavailable. Grabens displaying an inner central trough that form when significant withdrawal occurs (in wholly brittle crust under no or limited applied traction; see Figures 15 and 16) are especially useful. In the experiments the faults have changing dip angles with depth, in agreement with natural examples in which dip angle varies according to lithostatic pressure field [e.g., *Odonne et al.*, 1999]. For simplicity, if faults are assumed to be planar, then the depth of the deflating body is obtained from central trough width W_c, the graben width W_g, the brittle layer thickness e, and the drained area width B using relations

$$W_g = B + 2e/\tan\beta$$
$$W_c = B - 2e/\tan\alpha \tag{1}$$

where α is reverse fault dip and β normal fault dip. The system of equations (1) can be solved for e:

$$e = k\frac{W_g - W_c}{2} \tag{2}$$

where $k = (\tan\alpha \tan\beta)(\tan\alpha + \tan\beta)$. In the experiments, commonly found mean dip angles are $\alpha \approx 85$ and $\beta \approx 50$, suggesting an approximation for equation (2):

$$e \approx 0.54(W_g - W_c) \tag{3}$$

Combining equations (1) and (2) shows that B and e can be calculated separately:

$$B = \frac{W_g + W_c}{2} - k'\frac{W_g - W_c}{2} \tag{4}$$

where $k' = (\tan\alpha - \tan\beta)(\tan\alpha + \tan\beta)$. Using $\alpha \approx 85$ and $\beta \approx 50$,
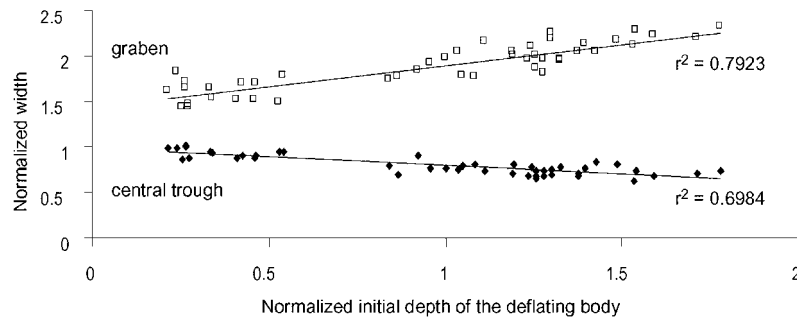
$$B \approx 0.094W_g + 0.91W_c \tag{5}$$

Figure 16. Width of collapse troughs and grabens versus initial depth of deflated body (balloon) in pure deflation experiments with no silicone layer. Values are normalized to balloon diameter.
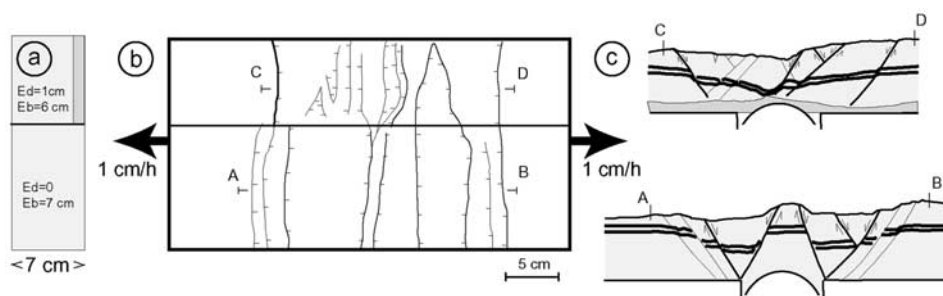
Figure 17. Results of scaled horizontal traction experiments (rate 1 cm/h during 2h30') with no withdrawal: (a) rheologic cross section, (b) final surface view, and (c) final cross sections. Sequence of faulting: faults active at the end of experiment are displayed in bold; the earlier faults are displayed with thin lines.

Examples of the application of equations (3) and (5) to narrow grabens will be given below.

5.1.6. Sequence of Fracture Development and Collapse

[60] In withdrawal experiments in a brittle medium analog (with no horizontal traction; see Figure 15, AB), the collapse trough initiates after 15–35% withdrawal and is followed by outward propagation of stepping normal faults on both trough sides. After 45–65% withdrawal the maximum breadth of the deformed area is attained and the whole strain is achieved by slipping along the outermost border faults. Conversely, in horizontal traction experiments in a brittle analog medium (Figure 17, AB), once lateral grabens have synchronously initiated then deformation migrates inward by activation of new faults between the outermost normal faults.

[61] In brittle ductile analog experiments in which conjugate grabens are created (Figure 15, CD, and Figure 18) the lateral grabens form in response to inward ductile flow before central collapse occurs. No preferential fault development sequence has been found in ductile analog experiments (Figure 17, CD).

5.1.7. Interpretation of a Ductile Layer in Experimental Models

[62] Experimental results emphasize that the presence of a ductile layer between the magma body and the upper brittle crust tends to increase surface strain distribution (Figures 19a, 19c, and 19e), which is in agreement with many earlier studies showing that strain distribution depends on brittle crust thickness [e.g., *Vendeville et al.*, 1987; *Allemand and Brun*, 1991]. In experimental models including a ductile layer in which twin grabens are observed to form, the location of the grabens is related to the width of the groove and to the ductile layer thickness. In pure extension experiments, a very thin or absent ductile layer must be imposed to generate two conjugate grabens (Figure 19b), whose bounding faults are rooted at the edges of the groove. Therefore, in this case, graben location directly depends upon groove width. The zone comprised between the fault anchor points represent a null deformation area equivalent in the wild to a stress free boundary that does not transmit lithospheric stresses. Along an oceanic ridge axis, a magma lens located at the upper part of a magma reservoir (or a ductile lower crust) may behave this way [*Chen and Morgan*, 1990; *Goff*, 1991; *Shaw and Lin*, 1996; *Eberle and Forsyth*, 1998]. Therefore the experimental models containing a ductile layer may be compared to either a brittle ductile crustal rheology, or a brittle crust rheology, provided that the magma reservoir is capped with a magma lens.

5.1.8. Surface Evidence of Magma Withdrawal Direction

[63] In deflation experiments, lateral liquid migration during withdrawal produces V-shaped normal fault traces around the collapse trough, with the V tip oriented toward the direction of drainage. Similar patterns are observed at propagating oceanic ridges during along-axis melt lens migration at the top of a crustal reservoir [*Hey et al.*, 1989]. Their formation mechanism remains poorly under-
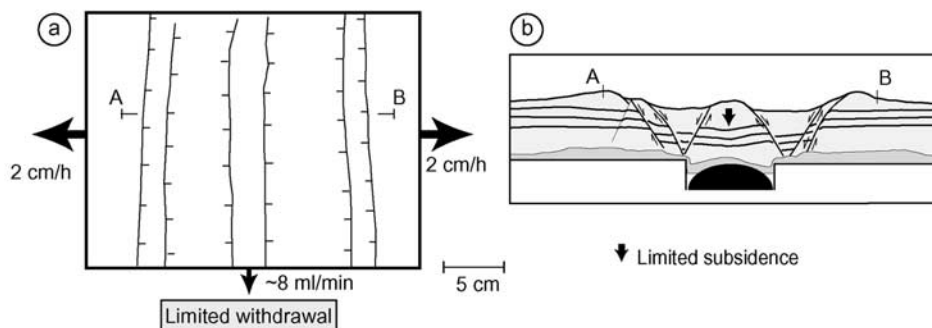

Figure 18. Results of a scaled experiment combining simultaneous extension and limited withdrawal: (a) final surface view and (b) final cross section. Further withdrawal induces subsequent collapse trough formation in a way similar to deflation experiments with no horizontal traction.
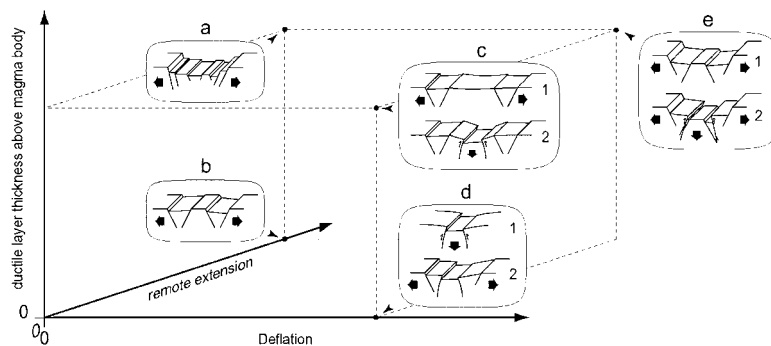
Figure 19. Synthesis of surface structures expected from the experimental results of graben and collapse trough development as a function of deflation, remote stress field, and ductile crust thickness above the reservoir. Lower fault tips are not displayed. Numbers refer to the sequence of events. Arrows indicate the main direction of displacement.

stood, however the experimental results reported here suggest that V-shaped fault trace may be interpreted as an indicator of magma flow, i.e., when a magma fraction in an overpressurized reservoir invades the fracture of a new ridge segment this results in a limited reservoir deflation.

5.1.9. Mass Wasting

[64] Landsliding is common to every deflation experiment because of the unstable hanging wall of the trough-bounding reverse faults. This was also been featured in other experiments [*Roche et al.*, 2000]. Trough broadening by mass wasting along fault scarps is thus a major mechanism of graben and trough evolution.

5.2. Application to Modified Narrow Grabens

[65] Modified grabens affected by collapse pits and troughs, U-shaped troughs, and narrow chasmata may be explained by several of the mechanisms described above.

5.2.1. Pit-and-Trough Chains

[66] Pit-and-trough chains may form by any mechanism provided that deflation occurs (Figures 19c–19e). Pit-and-trough chains not associated with grabens may result from limited deflation in a non/weakly deviatoric remote stress field (Figure 19d, 1). Those observed within a graben may form by continuing deflation (Figure 19d, 2) or in a stronger extensional stress field (Figure 19e, 2). Because of the uncertainty of surface interpretation arising from erosional processes and volcanic activity, and the absence of data for constraining heat flow when the tectonic structures formed, it is hard determining if the DBT was below or above the magma reservoir. Most chains of pits and troughs do not require the DBT to be higher than the top of the reservoir.

[67] Figure 20 shows examples of pit-and-trough chains within single grabens displaying inverse proportionality between graben width and the width of central pits and troughs. These examples match the experimental results in which deflation occurs in absence of remote extension and of a ductile layer between the deflating body and the surface. The observation that many pit-and-trough chains are not associated with grabens, is also in agreement with experiments in which graben formation occurs (Figure 19d, 2) only if deflation continues after the central collapse trough has formed (Figure 19d, 1). Equations (2) and (4) allow the estimation of depth and width of the deflating body in cases where the geometry of the central trough and the graben has

remained close to pristine. An idea of the depth and width may be given by application of equations (3) and (5). Applying these equations to the Noctis Labyrinthus example (Figure 20a) the depth of the top of the magma body is found to vary between 3.6 km and 6.7 km, and its width between 4.1 and 7.7 km. In the Alba Patera area (Figure 20b) they are found to be within the range 0.2–1 km, and 0.7–1.5 km respectively. In both cases these magma bodies are interpreted to be only the upper part of the magmatic plumbing feeding the flood lavas. The Noctis Labyrinthus example shows that subsequent deflation of a deeper magma body induces late stage and broader-scale collapse. This observation may be extrapolated to the whole Noctis Labyrinthus area, where the labyrinthus corridors (who display aligned pits and troughs), may connect deeper intrusions forming corridor intersections. The Noctis Labyrinthus plumbing system would then resemble that of extensional margins in hotspot setting, such as the North Atlantic volcanic province during the early history of the Tertiary Thulean mantle plume [*Callot et al.*, 2001].

5.2.2. Small Chasmata and Linear U-shaped Troughs

[68] Small chasmata are significantly wider and deeper than pits and troughs. Because of the one order of magnitude larger collapsed volume observed, small chasmata are thought to result from deflation of a larger and deeper magma body than the magma bodies inferred for pits and troughs. However, in detail the width and depth of the magma body cannot be estimated because initial depression geometry has been removed by wall erosion (see an example on Figure 21). Similarly, linear U-shaped troughs may not be used to infer magma body geometry at depth. The numerical approach, below, may nevertheless help constrain physical parameters for their formation.

[69] In areas where pit-and-trough chains and narrow chasmata are combined, two magma bodies may be required. The deepest level may be the NBZ or the DBT, whereas the shallowest may be a stress barrier at which upward propagating dikes turn to sills that gradually build a shallow depth magma chamber [e.g., *Gudmundsson*, 1990b].

5.2.3. Tectonic Patterns Involving Shallow Ductile Layer

[70] In many instances, observations at modified grabens are not inconsistent with interpretation of a shallow ductile
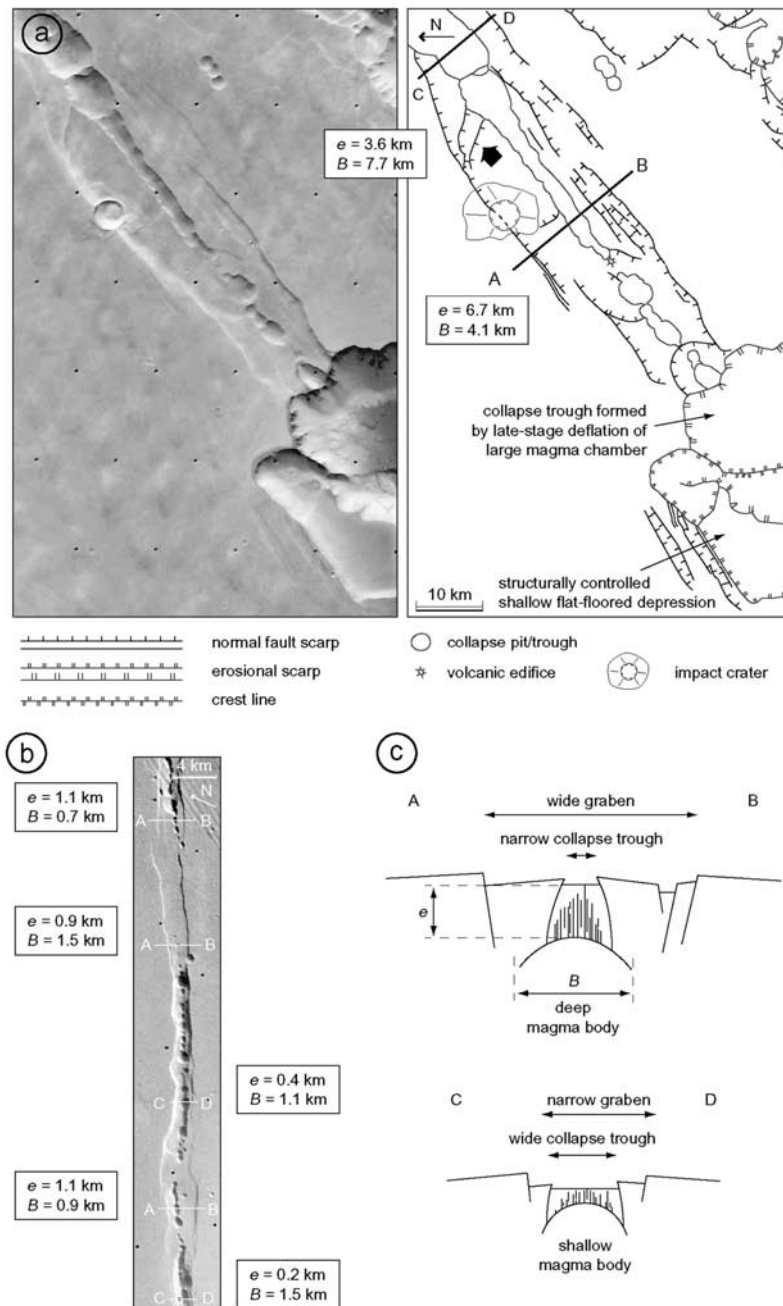
Figure 20. (a) Surface interpretation in southeast Noctis Labyrinthus. The arrow indicates direction of magma flow and graben propagation from the orientation of the two oblique normal faults nearby (see Figure 23). Part of NASA/JPL Viking Orbiter image 47A20 centered at 99.71°W, 10.14°S, 105 m/pixel. (b) Similar observations at Labeatis Fossae. NASA/JPL Viking Orbiter image 229A23, 52 m/pixel, 92.05°W, 24.12°N. (c) Schematic interpretations of profiles AB and CD in Figures 20a and 20b from experimental results in which deflation of a magma body occurs in a brittle crust with negligible remote extension (Figures 15 and 19d).

layer, or possibly a magma body that has undergone partial withdrawal only, but such a ductile level is not required. Existence of a ductile layer is expected to result in distributed strain. In general, the broadest modified narrow grabens and the chasmata have been extensively eroded and most clues to their geometry prior to erosion have been removed. Nevertheless, there are several examples where the observed strain distribution suggests existence of a shallow ductile layer. Twin grabens aligned with U-shaped trough and pit chains are not frequent but detailed analysis of MGS and Viking imagery has revealed examples in various areas of Mars, some of which are illustrated on Figures 22a, 22b, 22d, and 22e. On Figure 22c the geometry of a major regional graben system, Tempe Fossae, has been influenced by local stress fields, at least one of which have probably been induced by local magma centers. Strain
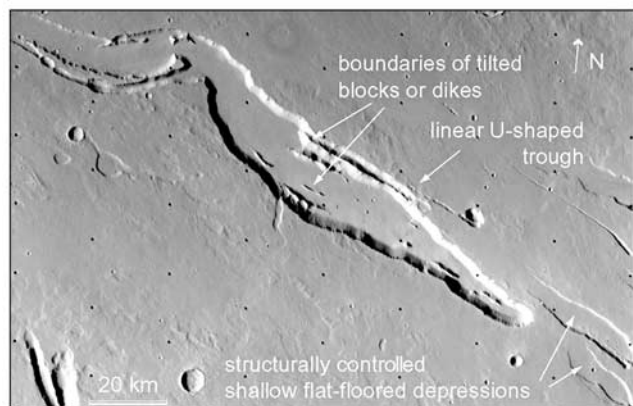
Figure 21. Shallow chasma in Elysium Fossae. Initial chasma structure remnants are observed within the chasma, but retrieving initial chasma geometry is much too speculative to be used to infer the geometry of subsurface magma body. Note that the internal structures may be interpreted as a series of tilted blocks aligned with the border faults observed southeast of the chasma. Initial chasma structure might be a wide rift developed in a crust having a shallow ductile layer. U-shaped troughs parallel to the chasma suggest existence of a dike or another linear magma body parallel to the magma body underneath the chasma but shallower. Part of NASA/JPL Viking Orbiter Image VO 541A24 centered at 220.02°W, 29.44°N, 152 m/pixel.

distribution over a broad area suggests existence of a shallow ductile layer, which is supported by results of rift flank uplift inversion and gives a ~ 10 km thick elastic lithosphere in this area [*Wilkins and Schultz*, 2001].

[71] Figure 21 shows a chasma from the Elysium Fossae that displays structural remnants suggestive of a distributed deformation event prior to extensive erosion. It demonstrates that despite present simple morphology, chasmata may have initiated as broad extensional systems that later underwent broad-scale collapse and wall retreat. Distributed deformation at chasmata may have resulted from deflation of a widespread underlying magma body mechanically acting as a ductile layer underneath the brittle crust.
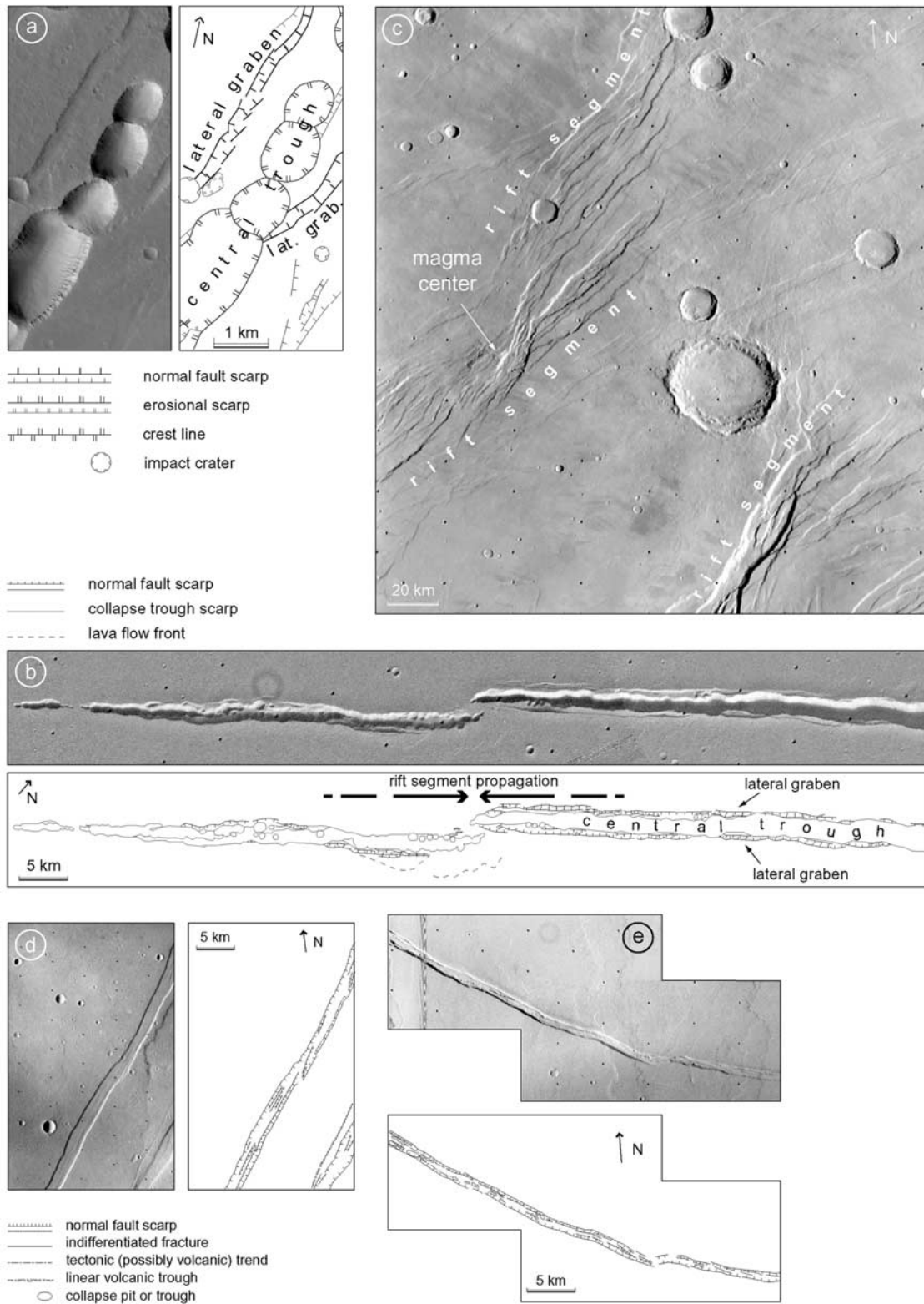
5.2.4. Direction of Magma Flow

[72] V-shaped fault profiles are observed in the Alba Patera and Noctis Labyrinthus areas. Figure 23 shows an example of a V-shaped fault profile at a Martian graben that may be interpreted as an indicator of magma flow during reservoir withdrawal. From analogy with terrestrial analogs at propagating rifts, this geometry might indicate the direction of magma propagation within the crust and graben opening. The magma body underlying the grabens is thought to have propagated from the Tharsis central area [*Mège and Masson*, 1996], which is in agreement with the orientation of the V tip. Another example can be found at the Noctis Labyrinthus given on Figure 20a.

5.3. Numerical Modeling of Withdrawn Magma Volume

[73] The magnitude of deflation that induced surface collapse may be numerically investigated by comparing the volume of the deflated magma and the volume of the void generated at surface. Figure 24 shows two end-members volume transfer mechanisms that are accounted for in the models. In a closed system, the whole magma body is the deflated lens, and there is no magma replenishment. In an open system, the magma lens is connected with a reservoir that begins replenishing as soon as significant magma underpressurization occurs (Figure 24). In the first step, limited crustal stretching traps magma at depth, which in turn leads to overpressure in the magma lens and helps focus tectonic strain at surface (step 1). Dike emplacement (not shown on Figure 24) occurs between the magma lens and the surface in such a way that the total dilation remains vertically constant. Gradually magma overpressure decreases (step 2). As long as magma pressure is positive, the erupted magma volume does not decrease the magma lens volume, and there is no surface collapse. When the magma pressure falls below zero, the differential stress in the host rock increases to a critical value σ_c equal to rock strength (step 3). Then the whole host rock body above σ_c fails and collapses into the deflated lens (step 4). The volume of the unstable host rock may be equal to the volume of the collapse trough that eventually forms at surface. In the closed system considered, the volume of destabilized host rock material as deduced from the volume of the surface trough is thus a direct measure of the deflation magnitude.

Figure 22. (opposite) Possible surface structures denoting shallow ductile layer. (a) Central trough surrounded by lateral grabens at Tractus Catena (part of MOC image M03-06623 centered at 101.26°W, 33.32°N, 3.04 m/pixel). This pattern is observed in experimental results when the top of the ductile layer lies above the top of the magma body (Figures 19c, 2, and 19e, 2). (b) The same at Labeatis Fossae (part of Viking Orbiter images 229A32-34 centered at 94.34°W, 22.33°N, 50 m/pixel). The geometry of rift segment tips gives direction of magma propagation [e.g., *Sempere and Macdonald*, 1986]. (c) Distributed stretching is also featured in shallow ductile layer experiments in extensional stress field (Figures 19a and 19e). Grabens at Tempe Fossae fanning around central volcanic edifice suggests existence of a shallow ductile layer during magmatic deflation [see, e.g., *McKenzie et al.*, 1992]. Viking Orbiter image 704B54 centered at 71.98°W, 38.05°N, 213 m/pixel. (d) Grabens displaying an internal horst are locally observed at Labeatis Fossae, northwest Figure 22b. A parallel graben of similar geometry displays central troughs, suggesting that the graben formed above a weakly deflating magma body while the remote stress was extensional (Figure 19e). Part of Viking Orbiter image 662A67 centered at 95.26°W, 22.59°N, 33 m/pixel. (e) Same observations at Gordii Fossae. Note in passing that the graben in the western part of the mosaic displays two major border faults and two internal pit-and-trough chains, which is not consistent with the hypothesis that the graben formed in response to the driving pressure of a single emplacing dike. Part of Viking Orbiter images 659A14 (124.51°W, 17.82°N) and 659A16 (124.48°W, 17.32°N), 40 m/pixel. MOC images by NASA/JPL/MSSS, Viking Orbiter images by NASA/JPL.

normal fault scarp
erosional scarp
crest line
impact crater

normal fault scarp
collapse trough scarp
lava flow front

normal fault scarp
indifferentiated fracture
tectonic (possibly volcanic) trend
linear volcanic trough
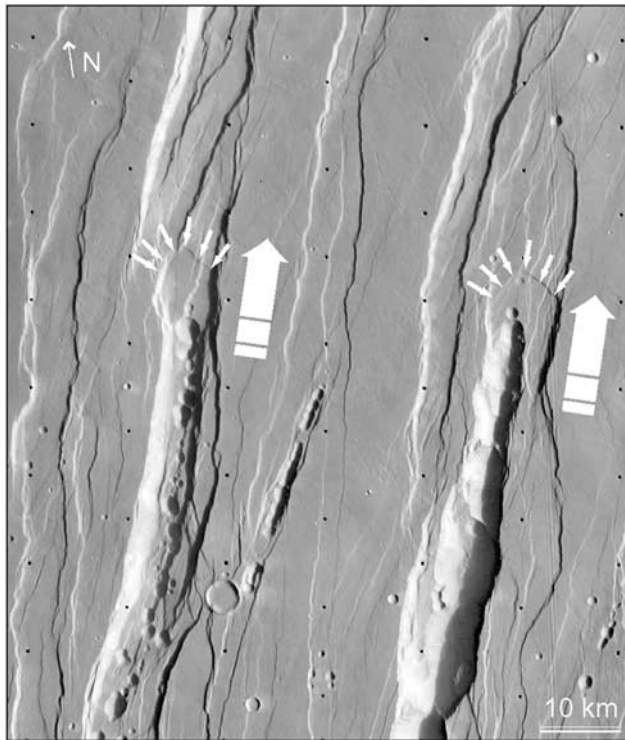**collapse pit or trough**

Figure 23. Direction of magma flow during magma withdrawal from orientation of oblique normal faults associated with modified graben formation. Another example is given in Figure 20a. Part of NASA/JPL Viking Orbiter image 253S52, 87 m/pixel, 106.16°W, 34.79°N.

If the magma body is being replenished, the volume of destabilized host rock, as deduced from the volume of surface trough, is an underestimate of the magnitude of deflation.

[74] In order to extrapolate surface trough volume to the volume of destabilized materials above the magma lens, the fraction of the measured trough volume that formed initially during the early tectonic stretching episode should be removed. However, the contribution of tectonic stretching is thought to be small/negligible compared with the volume created by volcanic collapse, both because strain estimates at unmodified narrow grabens shows very low strain [*Plescia*, 1991; *Golombek et al.*, 1994], and because part of the void created this way should have been filled by early lava flows (V_{el} on Figure 24).

[75] In the case of a single deflation event, the expected collapse mechanism is rapid stoping over the reservoir [*Roche et al.*, 2000]. However, in some cases the volume of the surface trough may result from successive withdrawal events, and the sum of the pressure drops equals the pressure drop in case of a single larger collapse event.

[76] In order to constrain the magnitude of underpressure P_m we use the trough volume data obtained from morphometric analysis of the DEMs (Table 1). We assume that the volume of the magma lens roof remains constant during surface collapse, and compute the magma underpressures using a boundary element code.

[77] First the extent (width B and length L) of the deflating part of the reservoir is defined assuming that it

is not larger than the extent of the bottom of the trough above (Table 2). Its shape is flat bottomed lens with a convex top aligned with the trough. This geometry is consistent with a buoyant magma generated by adiabatic decompression, or laterally flowing from a remote source region, and trapped at a rheological boundary below a slightly thinned brittle crust (Figure 25). In most cases its maximum thickness t is taken to be 1 km. This value is usually close to the minimum thickness required, for the volume that can be made available in the lens, to exceed the volume of the collapsing hot rock material. However, if magma reservoir replenishment occurs before the end of the collapse event then the volume of the reservoir may not be correlated with surface trough volume. In the Valles Marineris region, some reservoir thicknesses values, t, were taken to more than 1 km when taking 1 km resulted in magma underpressures that were so large that the magmatic processes involved might need to significantly differ from those in the other areas. The magnitude of the pressure drop is obtained at various depths e. For the most voluminous collapse troughs, thought to correspond to very deep reservoirs, e may be at the level of neutral buoyancy, 10 km [*Wilson and Head*, 1994]. Compute[3D] (Rocscience, Inc.) was selected for its ability at measuring the volume of host rock material below or beyond any stress.

[78] For a given reservoir size (L, B, t, e), the magma pressure P_m is initially set to the vertical stress. Then its magnitude is increased until the volume of the host rock, beyond the in situ rock strength, approximates the volume of the trough. The model consists of an elastic half-space subject to gravitational forces. Remote tectonic stress is set to 0 in order to visualize the structural effect of deflation alone. We investigate two extreme vertical stress conditions. In some experiments pore pressure P_p is assumed to be null. The vertical stress is thus ρge, where 3.72 m.s^{-2}, is taken to 2900 kg.m^{-3}, g = 3.72 m.s^{-2}, and e the depth of the top of the magma body. In other experiments we conducted, the pore pressure was considered to be as high as $\rho ge/2$ (Table 2). Based upon reasonable assumptions about the strength envelope of the Martian crust [*Banerdt et al.*, 1992], and with inferences of elastic lithosphere thickness on Mars from MOLA data [*Zuber et al.*, 2000], the ductile level that possibly exists in the deep crust is assumed to be deeper than the modeled part of the crust. Stress amplification induced by the possible existence of a ductile crust [*Kusznir and Bott*, 1977] is not taken into account. Young's modulus is taken to be 40 GPa and the friction angle is 30°. The computations are performed in a grid that covers one quarter of the model and extrapolated to the whole model. Node spacing is not a critical issue in the models because we are not interested in the details of the tectonic processes during subsidence, but on large-scale rock volumes. We found that >70,000 nodes are usually enough to obtain reasonably accurate results.

[79] We determined that the cumulated underpressure ΣP_m required to explain the trough volumes ranges between tens of MPa and 350 MPa, depending on pore pressure and reservoir size and depth. Figure 26 gives an example of a trough from the Calydon Fossae, SW of Valles Marineris, whose volume may be explained by this range of underpressures in a reservoir located at 5 km depth. For the smallest troughs the reservoir thickness
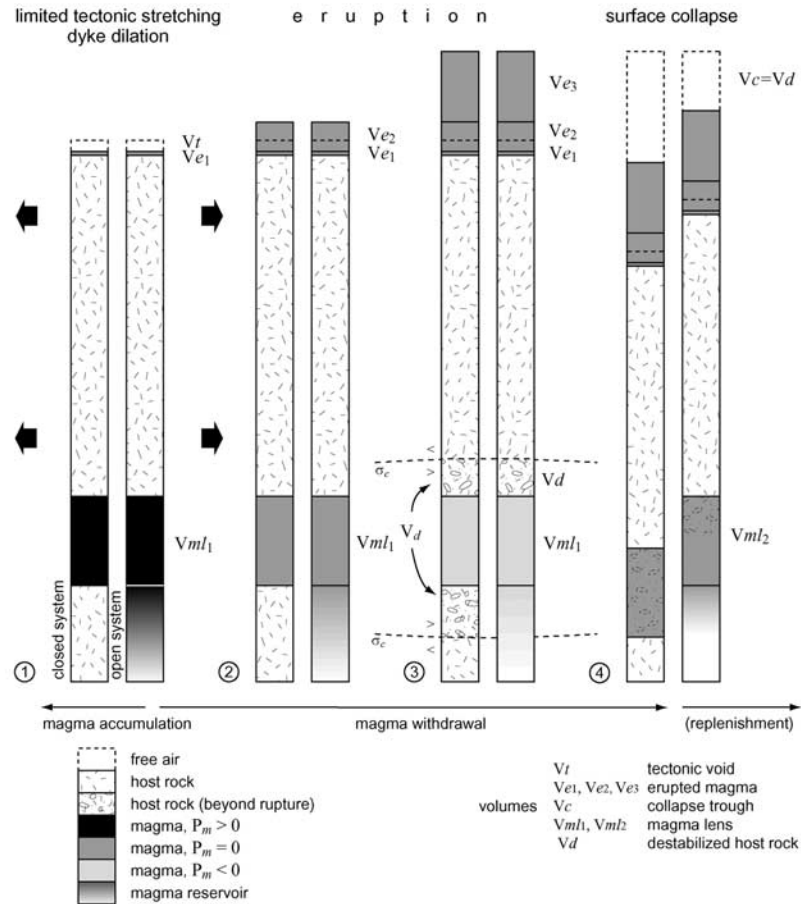
Figure 24. Volume transfers inducing surface collapse as modeled in the numerical experiments.

needs to be > 2 km for the volume of the host rock above failure not to exceed the volume of the reservoir and hence allow trough formation in a single collapse event with negligible reservoir replenishment. This results from the lower width/depth ratio for small troughs than for more voluminous troughs such as chasmata. The reservoir below the smallest measured trough (12 on Table 2) needs to be at >3–4 km thick. This is based upon the assumption that the reservoir width (top 1 km at the top, 2 km at the bottom) is on the order of the trough width (1 km). It would still require a reservoir at least 2 to 3 km thick if reservoir width 2 km (top) to 5 km (bottom).

6. Conclusion

[80] Ubiquitous pits and troughs at Martian grabens are shown to be key features for understanding the volcanic and tectonic graben evolution. Step by step, searching for their formation has lead to suggest a mechanism of graben evolution akin to volcanic tectonic models of terrestrial rifting. Using either MOLA data or combination of MOLA data and Viking Orbiter stereoscopic images, the volumes of removed material at individual troughs and chasmata are on the order of tens to hundreds of km^3. The volume of some small chasmata in the Tharsis and Elysium regions, thought to be of similar origin, probably attains one thousand km^3 or more. The volume of pit craters is smaller though not measurable using the current altimetry and topography data. The large volumes we found probably proscribe a mechanism of pressure drop above single dikes (or sinking in other mode I fractures), and make necessary emplacement and subsequent deflation of magma reservoirs beneath the grabens. The huge quantity of magma required to feed such reservoirs can be readily obtained by mantle adiabatic decompression and the thermal anomalies that have been involved in large Martian volcanic igneous provinces building [*Mège and Masson*, 1996; *Mège*, 2001], assuming that the present-day crustal thicknesses, 50 km on average [*Zuber et al.*, 2000], are not smaller than when the grabens and troughs formed. The reservoirs were trapped in the regions of ongoing tectonic thinning and have thus an elongated shape. Reservoir underpressurization, up to 350 MPa or more, is inferred from numerical simulation of reservoir deflation. These values may have been reached either by single catastrophic withdrawal events followed by stoping, or by successions of small-scale deflation events, for instance corresponding to dike emplacement. The depth of the reservoirs beneath the grabens displaying pits and troughs can be inferred from surface observations. We did not carry out a global survey, but in representative areas of Alba Patera and Noctis Labyrinthus we found that magma reservoirs might lie at ~1 km and ~5 km depth respectively, and have widths in the same range. Theoretical considerations based on neutral buoyancy zone modeling [*Wilson*

Table 2. Reservoir Parameters Consistent With Observed Trough Volumes[a]

N°	L, km	B, km	e, km	t, km	σ_c, MPa	P_p/P_l, MPa	ΣP_m, MPa	V_t, km³
1	75	5	5	1	53	0	−145	420
			5	1	26	0.5	−60	
			10	1	105	0	−235	
			10	1	53	0.5	−85	
2	8	2	2	1	21	0	−80	14
			2	1	10.5	0.5	−40	
			5	1	53	0	−170	
			5	1	26	0.5	−80	
3	40	5	5	1	53	0	−85	37
			5	1	26	0.5	−32	
			10	1	105	0	−130	
			10	1	53	0.5	−30	
4	40	5	5	1	53	0	−120	130
			5	1	26	0.5	−45	
			10	1	105	0	−190	
			10	1	53	0.5	−120	
5	30	5	5	1	53	0	−180	348
			5	1	26	0.5	−70	
			10	1	105	0	−300	
			10	1	53	0.5	−110	
6	30	5	5	1	53	0	−155	232
			5	1	26	0.5	−65	
			10	1	105	0	−260	
			10	1	53	0.5	−95	
7	20	5	5	1	53	0	−100	42
			5	1	26	0.5	−40	
			10	1	105	0	−160	
			10	1	53	0.5	−45	
8	13	1	2	2	21	0	−100	44
			2	2	10.5	0.5	−30	
			5	2	53	0	−140	
			5	2	26	0.5	−30	
10	20	5	5	1	53	0	−205	324
			5	1	26	0.5	−85	
			10	1	105	0	−345	
			10	1	53	0.5	−135	
11	20	10	5	1	53	0	−105	265
			5	1	26	0.5	−30	
			10	1	105	0	−170	
			10	1	53	0.5	−45	
12	10	2	5	4	53	0	−190	37
			5	4	26	0.5	−75	
			10	4	105	0	−315	
			10	4	53	0.5	−115	

[a]P_l: lithostatic pressure, P_p: pore pressure, ΣP_m: sum of the magma underpressures required for producing the observed trough volumes, σ_c: critical failure stress using the strength envelope for Mars given by *Banerdt et al.* [1992]. Magma underpressure accuracy is ±5 MPa.

and Head, 1994] suggest that 10 km should be another preferential depth for magma ponding. However, only an exhaustive graben and trough survey can determine whether preferential depths of magma body emplacement exist at Tharsis, Elysium, or global scale.

[81] Dike injection from the reservoirs is actually a reasonable means to channel the magma to the surface. This study confirms earlier studies suggesting that dike swarms should exist on Mars, but it is likely that every graben displaying aligned volcanic morphologic features should have its own dike swarm(s), for example, similar to the dikes in the Icelandic fissure swarms. Strictly speaking, these dike swarms are thus not akin to the terrestrial giant mafic dike swarms. They are shorter and probably thinner, and it is likely that a number of them, emplaced late in the reservoirs' history, carried acidic magmas differentiated in

the reservoirs. Also they are fed from below, in contrary to a number of giant dike swarms that appear to have been fed from central magma chambers [e.g., *Ernst and Baragar*, 1992]. Nevertheless, at the scale of the large igneous province they are observed in, they may be viewed as dikelets, and the feeding reservoirs may be viewed as equivalent to giant mafic dikes [*Ernst et al.*, 2001] and may have emplaced in part vertically (in response to mantle decompression) and in part laterally (channeling from the central part of the igneous province [*Thompson and Gibson*, 1991; *Sleep*, 1994b]). Magma propagation would occur at a speed depending on magma decompression and tectonic activity timescales, i.e., much lower than magma propagation in dikes [e.g., *Rubin*, 1995].

[82] Because of the difference in magma emplacement mechanism, there is little chance that the dikes have played a significant role in surface fracturing by way of magma pressure. This inference also applies to other terrestrial planets because it is based on detailed examination of terrestrial evidence and mechanical models in addition to Martian evidence. It is possible though that some dikes, as mechanical discontinuities, may have been involved in the location of surface fractures during the early phase of fracture initiation [see also *Koenig and Pollard*, 1998].

[83] Magmatic deflation not only explains the occurrence of pits and troughs in grabens, it may also contribute to the initiation and development of graben border faults. There might also be cases where volcanically modified grabens formed entirely in response to magmatic deflation with no influence of regional stress.

Appendix A: Method for the Calculation of Depression Volumes

[84] To measure the depressions we use two types of DEMs. The first type combines accuracy of MOLA altimetry data and spatial resolution of stereo-derived Viking DEMs (Figure 7). *Baratoux et al.* [2001] have described another method combining these two data sets. The second type is from extrapolation of MOLA data only. Such DEMs were used for studying collapse features in areas where there is no Viking stereo coverage or where the spatial resolution of Viking stereo derived DEMs would have been insufficient.

[85] In order to achieve a spatial resolution exceeding that of the currently available MOLA [*Smith et al.*, 2001] derived DEM (1/32° per pixel or ~1.864km/pixel), we needed to produce DEMs from stereo imagery yielding a spatial resolution of ~1.8 km/pixel or finer. In view of the requirement of our stereo matching software, "Gotcha" [*Day et al.*, 1992], that uses typically a correlation patch diameter of ~20 pixels for most areas on Mars, this limits potentially useful stereo pairs to images of <90 m/pixel resolution. A search was made in several sites displaying modified narrow grabens of major interest using a stereo coverage program [*Cook et al.*, 1992] for Viking Orbiter [*Snyder*, 1977] images; ten stereo pairs were found (Table 3). The first two pairs were selected because they were comparable in resolution to the 90 m/pixel threshold, the remaining pairs were chosen because they were well below the above threshold and covered the regions of interest. However, 627A21:627A04 and 627A23:627A02 were sub-
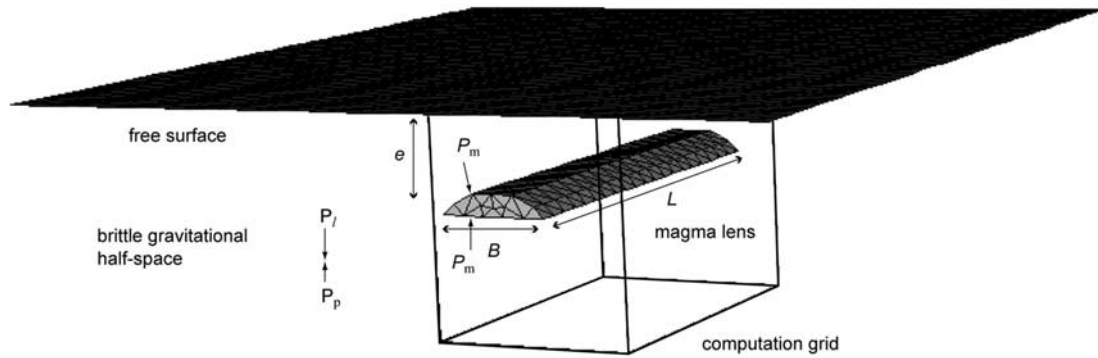
Figure 25. Geometric setting and the stress sources considered in the boundary element models.

sequently eliminated because of having too small an area of overlap. The theoretical height accuracy for a single matched point can be calculated using the formula from *Cook et al.* [1992]:

$$A = Max(I)\frac{C}{B/H} \qquad (A1)$$

where A is the theoretical height accuracy (m), Max (I) is the maximum resolution of either of the two images in a stereo pair (m), C is the precision to which image coordinate measurements can be made - assumed to be $C = 1.0$ for vidicon images, and B/H is stereo pair base separation to mean height ratio.

[86] The ability to resolve these theoretical relative heights depends upon how well the patch-based correlation matcher can lock onto surface texture. In the presence of poorly textured plains, or poor signal-to-noise ratio sections of images, image noise may increase C. On high contrast, high textured surfaces, C may be smaller and hence improve the ability to resolve finer heights. In addition, by combining many close point measurements together in a data bin, a finer height accuracy can be achieved. Therefore the theoretical height accuracy should be regarded as a means to compare and identify suitable stereo pairs. In comparison the 1/32° MOLA DEM, although constructed from individual MOLA points with absolute height accuracies of ±30 m and relative accuracies of ±0.3 m [*Smith et al.*, 2001], has been constructed by interpolating between MOLA points with an along track spacing of ∼330 m and an across track spacing of ∼1.8 km. Consequently the MOLA DEM will not have anywhere near the same relative and absolute height accuracy of individual altimeter points except on flat surfaces. Viking stereo DEMs have the advantage of more height points per unit area, albeit not of the same accuracy as individual MOLA points.

[87] The Viking Orbiter vidicon images were processed initially to correct geometrically for camera distortion, utilizing known reseau calibration mark positions [*Greeley and Batson*, 1990]. Next 10−20 manual tie points were
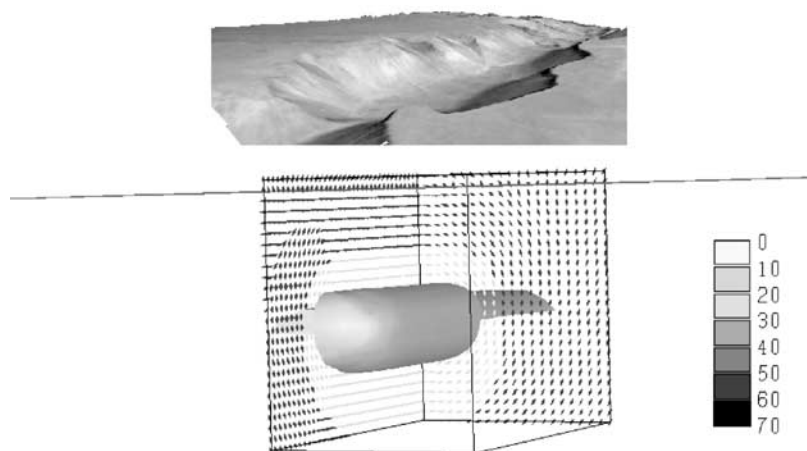

Figure 26. Example of deflation computation results for one of the Calydon Fossae troughs, SW of Valles Marineris (trough 10 in Tables 2 and 3). The gray levels give $\sigma_1 - \sigma_3$ for a model in which reservoir depth is 5 km and extends as long as the chasma extent. The grayscale does not apply to the stress arrows, which are almost everywhere between 0 and 30 MPa except close to the reservoir. Major arrow axis plane follows σ_1, and σ_3 is perpendicular to the arrow plane. The curved plane is differential stress isocontour 26 MPa, the stress level at which the host rock located near the top of the reservoir exceeds the strength envelope selected by *Banerdt et al.* [1992].

Table 3. Viking Orbiter Images Used in DEM Generation

Stereo Pair and Image Resolution in Parentheses	Theoretical Height Resolution of a Single Matched Point	Region Covered
062A71 (77 m): 044A28 (108 m)	200 m	92°–89°W, 5°–2°S
064A10 (80 m): 044A23 (107 m)	197 m	92°–89°W, 9°–6°S
627A21 (57 m): 627A02 (68 m)	330 m	
627A21 (57 m): 627A04 (68 m)	283 m	
627A23 (60 m): 627A02 (68 m)	375 m	
627A23 (60 m): 627A04 (68 m)	316 m	89°–84°W, 36°–89°N
627A25 (56 m): 627A04 (68 m)	358 m	
627A25 (56 m): 627A06 (67 m)	302 m	
627A27 (56 m): 627A06 (67 m)	340 m	
627A29 (56 m): 627A08 (67 m)	326 m	
627A29 (56 m): 627A10 (67 m)	279 m	

found in order to define an affine transform between each of the two images in a stereo pair. For stereo matching the images we utilized a semiautomated patch-based digital stereo matcher "Gotcha" from University College London [*Day et al.*, 1992]. The matcher finds for each pixel in the overlap region in the left image a corresponding pixel location in the right image. The matched points are next passed through a stereo intersection camera model to convert stereo pixel coordinates for each pair into longitude/latitude/height points, i.e., a Digital Terrain Model (DTM). The best available camera positions and orientations derived from previous photogrammetric adjustments of images [*Wu and Schafer*, 1984; *Davies*, 1978; *Eliason et al.*, 1999] are used in this stereo camera model. To optimize for the best spatial resolution, each image pair is stereo matched 12 times with correlation patch sizes of between 12 and 1 pixel radii. A large patch size has the greatest number of pixels to correlate on and is the least affected by image noise, however a large patch size yields a blurred DEM. A small patch size correlates less well when image noise is present, resulting in more topographic noise, but will yield sharper DEMs. To optimize highest DEM spatial resolution and the least noise, the DTMs generated are placed into a data cube with the Z axis corresponding to patch size and X and Y values corresponding to image sample and line coordinates in the left image [*Cook et al.*, 2000]. For each pixel in the left image, the corresponding height value is tracked from large patch size to small patch size until a reversal in height direction is observed, at which point the previous height value is output into the resultant DTM.

[88] Finally, in order to correct for height and/or position offsets and DTM tilts, each DTM is fitted to underlying MOLA 1/32° gridded DEM absolute height profiles by performing a photogrammetric adjustment using an approximation for offset and tilt fit [*Cook et al.*, 2000; *Craddock et al.*, 2001]:

$$H' = (\text{lon} + d\text{lon})a + (\text{lat} + d\text{lat})b + c + H \qquad (A2)$$

where H is the original DTM height (m) at a given longitude and latitude, a, b, c are tilt and offset parameters, and H' is the corrected height (m). $d$lon and $d$lat are stepped through incrementally in units corresponding to 1/128° on the surface. The correct values for $d$lon and $d$lat are obtained when the DEM has the closest fit to the MOLA DEM. A DEM mosaic is generated by binning and

averaging all available fitted DTM points within 1/128° × 1/128° pixels.

References

Allemand, P., and J.-P. Brun, Width of continental rifts and rheological layering of the lithosphere, *Tectonophysics*, *188*, 63–69, 1991.

Angelier, J., F. Bergerat, O. Dauteuil, and T. Villemin, Effective tension-shear relationships in extensional fissure swarms, axial rift zone of northeastern Iceland, *J. Struct. Geol.*, *19*, 673–685, 1997.

Antoniadi, E. M., *La Planète Mars: Map of Albedo Features of Mars*, 239 pp., Hermann and Cie, Paris, France, 1930.

Audin, L., I. Manighetti, P. Tapponnier, F. Métivier, E. Jacques, and P. Huchon, Fault propagation and climatic control of sedimentation on the Ghoubbet rift floor: Insights from the Tadjouraden cruise in the western Gulf of Aden, *Geophys. J. Int.*, *144*, 391–413, 2001.

Baer, G., Fracture propagation and magma flow in segmented dykes: Field evidence and fabric analyses, Makhtesh Ramon, Israel, in *Physics and Chemistry of Dykes*, edited by G. Baer and A. Heimann, pp. 125–140, A. A. Balkema, Brookfield, Vt., 1995.

Banerdt, W. B., and M. P. Golombek, Tectonics of the Tharsis region of Mars: Insights from MGS topography and gravity (abstract), *Lunar Planet. Sci. Conf.* [CD-ROM], *XXXI*, abstract 2038, 2000.

Banerdt, W. B., M. P. Golombek, and K. L. Tanaka, Stress and tectonics on Mars, in *Mars*, edited by W. S. Kiefer et al., pp. 249–297, Univ. Ariz. Press, Tucson, 1992.

Baratoux, D., C. Delacourt, and P. Allemand, High-resolution digital elevation models derived from Viking Orbiter images: Method and comparison with Mars Orbiter Laser altimetry data, *J. Geophys. Res.*, *106*, 32,927–32,941, 2001.

Best, M. G., and E. H. Christiansen, *Igneous Petrology*, 458 pp., Blackwell Sci., Malden, Mass., 2001.

Bonafede, M., and M. Olivieri, Displacement and gravity anomaly produced by a shallow vertical dyke in a cohesionless medium, *Geophys. J. Int.*, *123*, 639–652, 1995.

Boudier, F., and A. Nicolas, Magma chambers in the Oman ophiolite; fed from the top and bottom, *Earth Planet. Sci. Lett.*, *144*, 6959–6982, 1996.

Bruce, P. M., and H. E. Huppert, Solidification and melting along dykes by the laminar flow of basaltic magma, in *Magma Transport and Storage*, edited by M. P. Ryan, pp. 87–101, John Wiley, New York, 1990.

Burov, E. B., and L. Guillou-Frottier, Thermomechanical behavior of large ash flow calderas, *J. Geophys. Res.*, *104*, 23,081–23,109, 1999.

Callot, J.-P., L. Geoffroy, C. Aubourg, J.-P. Pozzi, and D. Mège, Magma flow directions of shallow dykes from the East Greenland volcanic margin inferred from magnetic fabric studies, *Tectonophysics*, *335*, 313–329, 2001.

Carr, M. H., and R. Greeley, Volcanic features of Hawaii, a basis for comparison with Mars, *NASA Spec. Publ., SP-403*, 211 pp., 1980.

Cattermole, P., Linear volcanic features at Alba Patera, Mars—Probable spatter ridges, *J. Geophys. Res.*, *91*, 159–165, 1986.

Cattermole, P., *The Story of the Red Planet*, 224 pp., Chapman and Hall, New York, 1992.

Cayol, V., J. H. Dieterich, A. T. Okamura, and A. Miklius, High rates of flank deformation prior to the 1983 eruption of Kilauea, Hawaii, *Science*, *288*, 2343–2346, 2000.

Chadwick, W. W., Jr., and R. W. Embley, Graben formation associated with recent dike intrusions and volcanic eruptions on the mid-ocean ridge, *J. Geophys. Res.*, *103*, 9807–9825, 1998.

Chen, Y., and W. J. Morgan, A non linear rheology model for mid-ocean ridge axis topography, *J. Geophys. Res.*, *95*, 17,583–17,604, 1990.

Cook, A. C., T. Day, J.-P. Muller, J. C. Iliffe, D. A. Rothery, G. D. Thornhill, and J. B. Murray, A Prolog-based Mars information system, *International Archives of Photogrammetry, Remote Sensing and Spatial Information Sciences*, vol. 17, pp. 788–794, RICS Books, Coventry, U. K., 1992.

Cook, A. C., D. Mège, and R. A. Craddock, Stereo derived digital elevation models of Mars fitted to MOLA profiles, *Lunar Planet. Sci. Conf.* [CD-ROM], *XXXI*, abstract 2008, 2000.

Craddock, R. A., G. A. Franz, A. C. Cook, and A. D. Howard, High resolution morphometric studies of Martian valley networks in the Iapygia region, *Lunar Planet. Sci. Conf.* [CD-ROM], *XXXII*, abstract 1833, 2001.

Dauteuil, O., J. Angelier, F. Bergerat, S. Verrier, and T. Villemin, Deformation partitioning inside a fissure swarm of the northern Icelandic rift, *J. Struct. Geol.*, *23*, 1359–1372, 2001.

Davies, M. E., F. Y. Katayama, and J. A. Roth, Control net of Mars, *NASA Rep., R-2309*, 91 pp., 1978.

Davis, P. A., K. L. Tanaka, and M. P. Golombek, Topography of closed depressions, scarps, and graben in the North Tharsis region of Mars: Implications for shallow crustal discontinuities and graben formation, *Icarus*, *114*, 403–422, 1995.

Day, T., T. A. C. Cook, and J.-P. Muller, Automated digital topographic mapping techniques for Mars, *International Archives of Photogrammetry, Remote Sensing and Spatial Information Sciences*, vol. 17, pp. 801–808, RICS Books, Coventry, U. K., 1992.

Delaney, P. T., Rapid intrusion of magma into wet rock: Groundwater flow due to pore pressure increases, *J. Geophys. Res.*, *87*, 7739–7756, 1982.

Delaney, P. T., D. D. Pollard, J. I. Ziony, and E. H. McKee, Field relations between dikes and joints: Emplacement processes and paleostress analysis, *J. Geophys. Res.*, *91*, 4920–4938, 1986.

Dilek, Y., M. E. Moores, and H. Furnes, Structure of modern oceanic crust and ophiolites and implications for faulting and magmatism at oceanic spreading centers, in *Faulting and Magmatism at Mid-Ocean Ridges*, *Geophys. Monogr. Ser.*, vol. 106, edited by W. R. Buck et al., pp. 219–265, AGU, Washington, D. C., 1998.

Doubre, C., L. Dorbath, I. Manighetti, E. Jacques, and L. Geoffroy, Current magmato-tectonic activity in the Asal-Ghoubbet Rift (Afar depression), Republic of Djibouti, *Eos Trans. AGU*, *82*, Fall Meeting Suppl., T51B-0869, 2001.

Durand, C., P. Gente, and O. Dauteuil, Caractéristiques morphologiques des segments axiaux le long de la dorsale médio-atlantique, *C. R. Acad. Sci., Part II*, *320*, 411–418, 1995.

Eberle, M. A., and D. W. Forsyth, An alternative, dynamic model of the axial topographic high at fast spreading ridges, *J. Geophys. Res.*, *103*, 12,309–12,320, 1998.

Ebinger, C. J., and N. H. Sleep, Cenozoic magmatism throughout East Africa resulting from impact of a single plume, *Nature*, *395*, 788–791, 1998.

Eliason, E., P. A. Garcia, A. Bennett, and C. E. Isbell, *Mars Mosaicked Digital Image Model (MDIM) and Digital Terrain Model (DTM)* [CD-ROM], vol. 15, U.S. Geol. Surv., Flagstaff, Ariz., 1999.

Elsworth, D., and B. Voight, Evaluation of volcano flank instability triggered by dyke intrusion, in *Volcano Instability on the Earth and Other Planets*, edited by W. J. McGuire, A. P. Jones, and J. Neuberg, *Geol. Soc. Spec. Publ.*, *110*, 45–53, 1996.

Ernst, R. E., and W. R. A. Baragar, Evidence from magnetic fabric for the flow pattern in the Mackenzie giant radiating dyke swarm, *Nature*, *356*, 511–513, 1992.

Ernst, R. E., K. L. Buchan, and H. C. Palmer, Giant dyke swarms: Characteristics, distribution and geotectonic applications, in *Physics and Chemistry of Dykes*, edited by G. Baer and A. Heimann, pp. 3–21, A. A. Balkema, Brookfield, Vt., 1995.

Ernst, R. E., K. L. Buchan, and H. C. Palmer, Diabase (dolerite) dyke swarms of the world, scale 1:35,000,000, *Open File Geol. Surv. Can., 3241*, 104 pp., 1996.

Ernst, R. E., E. B. Grosfils, and D. Mège, Giant mafic dyke swarms on Earth, Venus and Mars, *Annu. Rev. Earth Planet. Sci.*, *29*, 489–534, 2001.

Fialko, Y. A., and A. M. Rubin, Thermal and mechanical aspects of magma emplacement in giant dike swarms, *J. Geophys. Res.*, *104*, 23,033–23,049, 1999.

Forslund, T., and A. Gudmundsson, Crustal spreading due to dikes and faults in southwest Iceland, *J. Struct. Geol.*, *13*, 443–457, 1991.

Garcia, M. O., and M. G. Davis, Submarine growth and internal structure of ocean island volcanoes based on submarine observatiobs of Mauna Loa volcano, Hawaii, *Geology*, *29*, 163–166, 2001.

Garel, E., Modèles analogiques de l'évolution volcano-tectonique de l'axe de la dorsale ultra-rapide du Pacifique, DEA thesis, 79 pp., Univ. é de Bretagne Occidentale, Brest, France, 1998.

Garel, E., O. Dauteuil, and Y. Lagabrielle, Deformation processes at fast to ultra-fast oceanic spreading axes: Mechanical approach, *Tectonophysics*, *346*, 223–246, 2002.

Goff, J. A., A global and regional analysis of near ridge abyssal hill morphology, *J. Geophys. Res.*, *96*, 21,713–21,737, 1991.

Golombek, M. P., Structural analysis of lunar graben and the shallow crustal structure of the Moon, *J. Geophys. Res.*, *84*, 4657–4666, 1979.

Golombek, M. P., K. L. Tanaka, D. J. Chadwick, B. J. Franklin, and P. A. Davis, Extension across Tempe Terra and Sirenum provinces on Mars from measurements of fault scarp widths, *Lunar Planet. Sci. Conf.*, *XXV*, 443–444, 1994.

Greeley, R., Basaltic "plains" volcanism, in *Volcanism of the Eastern Snake River Plain, Idaho: A Comparative Planetary Geology Guidebook*, edited by R. Greeley and J. S. King, *NASA Contract. Rep., CR-154621*, 23–44, 1977a.

Greeley, R., Aerial guide to the geology of the central and eastern Snake River Plain, in *Volcanism of the Eastern Snake River Plain, Idaho: A Comparative Planetary Geology Guidebook*, edited by R. Greeley and J. S. King, *NASA Contract. Rep., CR-154621*, 59–111, 1977b.

Greeley, R., and R. M. Batson, *Planetary Mapping*, 196 pp., Cambridge Univ., New York, 1990.

Greeley, R., and J. E. Guest, Geologic map of the eastern equatorial region of Mars, scale 1:15,000,000, *U.S.Geol. Surv. Misc. Invest. Ser.*, *I-1802-B*, 1987.

Greeley, R., and P. H. Schultz, Possible planetary analogs to Snake River plain basalt features, in *Volcanism of the Eastern Snake River Plain, Idaho: A Comparative Planetary Geology Guidebook*, edited by R. Greeley and J. S. King, *NASA Contract. Rep., CR-154621*, 233–251, 1977.

Greeley, R., E. Theilig, and J. S. King, Guide to the geology of King's Bowl lava field, in *Volcanism of the Eastern Snake River Plain, Idaho: A Comparative Planetary Geology Guidebook*, edited by R. Greeley and J. S. King, *NASA Contract. Rep., CR-154621*, 171–188, 1977.

Grosfils, E., and J. W. Head, The global distribution of giant radiating dike swarms on Venus: Implications for the global stress state, *Geophys. Res. Lett.*, *21*, 701–704, 1994a.

Grosfils, E., and J. W. Head, Emplacement of a radiating dike swarm in western Vinmara Planitia, Venus: Interpretation of the regional stress field orientation and subsurface magmatic configuration, *Earth Moon Planets*, *66*, 153–171, 1994b.

Gudmundsson, A., Tectonic aspects of dykes in northwestern Iceland, *Jökull*, *34*, 81–96, 1984.

Gudmundsson, A., Dyke emplacement at divergent plate boundaries, in *Mafic Dykes and Emplacement Mechanisms*, edited by A. J. Parker, P. C. Rickwood, and D. H. Tucker, pp. 47–62, A. A. Balkema, Brookfield, Vt., 1990a.

Gudmundsson, A., Emplacement of dikes, sills and crustal magma chambers at divergent plate boundaries, *Tectonophysics*, *176*, 257–275, 1990b.

Gudmundsson, A., Formation and growth of normal faults at the divergent plate boundary in Iceland, *Terra Nova*, *4*, 464–471, 1992.

Gudmundsson, A., The geometry and growth of dykes, in *Physics and Chemistry of Dykes*, edited by G. Baer and A. Heimann, A. A. Balkema, pp. 23–34, Brookfield, Vt., 1995a.

Gudmundsson, A., Infrastructure and mechanics of volcanic systems in Iceland, *J. Volcanol. Geotherm. Res.*, *64*, 1–25, 1995b.

Head, J. W., III, and L. Wilson, Magma reservoirs and neutral buoyancy zones on Venus: Implications for the formation and evolution of volcanic landforms, *J. Geophys. Res.*, *97*, 3877–3903, 1992.

Head, J. W., III, and L. Wilson, Lunar graben formation due to near-surface deformation accompanying dike emplacement, *Planet. Space Sci.*, *41*, 719–727, 1994.

Hey, R. N., J. M. Sinton, and F. K. Duennebier, Propagating rifts and spreading centers, *The Geology of North America*, vol. N, *The Eastern Pacific Ocean and Hawaii*, edited by E. L. Winterer, D. M. Hussong, and R. W. Decker, pp. 161–176, Geol. Soc. of Am., Boulder, Colo., 1989.

Hoek, J. D., Mafic dykes of the Vestfold Hills, East Antarctica. An analysis of the emplacement mechanism of tholeiitic dyke swarms and of the role of dyke emplacement during crustal extension, Ph.D. thesis, 133 pp., Univ. of Utrecht, Utrecht, Neth., 1994.

Hoek, J. D., Dyke propagation and arrest in Proterozoic tholeiitic dyke swarms, Vestfold Hills, East Antarctica, in *Physics and Chemistry of Dykes*, edited by G. Baer and A. Heimann, pp. 79–93, A. A. Balkema, Brookfield, Vt., 1995.

Hubbert, M. K., Theory of scale models as applied to the study of geologic structures, *Geol. Soc. Am. Bull.*, 48, 1459–1520, 1937.

Kappel, E. S., and W. B. F. Ryan, Volcanic episodicity and a non-steady state rift valley along the northeast Pacific spreading center: Evidence from SeaMARC I, *J. Geophys. Res.*, 91, 13,925–13,940, 1986.

Karlo, J., Basaltic "plains" volcanism, in *Volcanism of the Eastern Snake River Plain, Idaho: A Comparative Planetary Geology Guidebook*, edited by R. Greeley and J. S. King, *NASA Contract. Rep.*, CR-154621, 121–131, 1977.

Kiefer, W. S., Magma production and mantle convection on Mars, *Lunar Planet. Sci. Conf.* [CD-ROM], XXXI, abstract 1527, 2000.

Koenig, E., and D. D. Pollard, Mapping and modeling of radial fracture patterns, *J. Geophys. Res.*, 103, 15,183–15,202, 1998.

Kumarapeli, S. P., K. St. Seymour, A. Fowler, and H. Pintson, The problem of the magma source of a giant radiating mafic dyke swarm in a failed arm setting, in *Mafic Dykes and Emplacement Mechanisms*, edited by A. J. Parker, P. C. Rickwood, and D. H. Tucker, pp. 163–171, A. A. Balkema, Brookfield, Vt., 1990.

Kusznir, N. J., and M. H. P. Bott, Stress concentration in the upper lithosphere caused by underlying viscoelastic creep, *Tectonophysics*, 43, 247–256, 1977.

Lagabrielle, Y., and M.-H. Cormier, Formation of large summit troughs along the East Pacific Rise as collapse calderas: An evolutionary model, *J. Geophys. Res.*, 104, 12,971–12,988, 1999.

Lagabrielle, Y., E. Garel, O. Dauteuil, and M.-H. Cormier, Extensional faulting and caldera collapse in the axial region of fast spreading ridges: Analog modeling, *J. Geophys. Res.*, 106, 2005–2016, 2001.

Le Dain, Y., B. Robineau, and P. Tapponnier, Les effets tectoniques de l'événement sismique et volcanique de novembre 1978 dans le rift d'Asal-Ghoubbet, *Bull. Soc. Geol. Fr.*, 22, 817–822, 1979.

Lister, J. R., and R. C. Kerr, Fluid-mechanical models of crack propagation and their application to magma transport in dykes, *J. Geophys. Res.*, 96, 10,049–10,077, 1991.

Liu, S. Y., and L. Wilson, Collapse pits due to gas release from shallow dikes on Mars, *Lunar Planet. Sci. Conf.* [CD-ROM], XXXI, abstract 1602, 1998.

Lonsdale, P., Structural geomorphology of a fast-spreading rise crest: The East Pacific Rise near 3°25′S, *Mar. Geophys. Res.*, 3, 251–293, 1977.

Macdonald, K. C., and P. J. Fox, The axial summit graben and cross-sectional shape of the East-Pacific Rise as indicators of axial magma chambers and recent volcanic eruptions, *Earth Planet. Sci. Lett.*, 88, 119–131, 1988.

Manighetti, I., P. Tapponnier, P.-Y. Gillot, E. Jacques, V. Courtillot, O. Armijo, J.-C. Ruegg, and G. King, Propagation of rifting along the Arabia-Somalia plate boundary: Into Afar, *J. Geophys. Res.*, 103, 4947–4974, 1998.

Mastin, L. G., and D. D. Pollard, Surface deformation and shallow dike intrusion processes at Inyo craters, Long Valley, California, *J. Geophys. Res.*, 93, 13,221–13,235, 1988.

McEwen, A. S., M. C. Malin, M. H. Carr, and W. K. Hartmann, Voluminous volcanism on early Mars revealed in Valles Marineris, *Nature*, 397, 584–586, 1999.

McGetchin, T. R., and G. W. Ullrich, Xenoliths and diatremes with inferences for the Moon, *Mars, and Venus, J. Geophys. Res.*, 78, 1833–1853, 1973.

McGill, G. E., and A. W. Stromquist, The graben in Canyonlands National Park, Utah: Geometry, mechanics, and kinematics, *J. Geophys. Res.*, 84, 4547–4563, 1979.

McKenzie, D., J. M. McKenzie, and R. S. Saunders, Dike emplacement on Venus and on Earth, *J. Geophys. Res.*, 97, 15,977–15,990, 1992.

Mège, D., Uniformitarian plume tectonics: The post-Archean Earth and Mars, in *Mantle Plumes: Their Identification Through Time*, edited by R. E. Ernst and K. L. Buchan, *Geol. Soc. Am. Spec. Pap.*, 352, 141–164, 2001.

Mège, D., and R. E. Ernst, Contractional effects of mantle plumes on Earth, Mars and Venus, in *Mantle Plumes: Their Identification Through Time*, edited by R. E. Ernst and K. L. Buchan, *Geol. Soc. Am. Spec. Pap.*, 352, 103–140, 2001.

Mège, D., and P. Masson, A plume tectonics model for the Tharsis province, Mars, *Planet. Space Sci.*, 44, 1499–1546, 1996.

Mège, D., and P. Masson, Tension fracturing at Uranius Fossae, Mars, *Lunar Planet Sci. Conf.*, XXVIII, 931–932, 1997.

Mège, D., Y. Lagabrielle, E. Garel, M.-H. Cormier, and A. C. Cook, Collapse features and narrow graben on Mars and Venus: Dike emplacement and deflation of underlying magma chamber, *Lunar Planet. Sci. Conf.* [CD-ROM], XXXI, abstract 1854, 2000.

Melosh, H. J., and C. A. Williams Jr., Mechanics of graben formation in crustal rocks: A finite element analysis, *J. Geophys. Res.*, 94, 13,961–13,973, 1989.

Merle, O., and A. Borgia, Scaled experiments of volcanic spreading, *J. Geophys. Res.*, 101, 13,805–13,817, 1996.

MOLA Science Team, paper presented at First Mars Global Surveyor Science Press Conference, Jet. Propul. Lab., Pasadena, Calif., 1997. (Available at mars.jpl.nasa.gov/mgs/sci/mola/data1/mola_first.html)

Montési, L. G. J., Concentric dike swarms on the flanks of Pavonis Mons: Implications for the evolution of Martian shield volcanoes and mantle plumes, in *Mantle Plumes: Their Identification Through Time*, edited by R. E. Ernst and K. L. Buchan, *Geol. Soc. Am. Spec. Pap.*, 352, 165–181, 2001.

Morgan, J. K., G. F. Moore, D. J. Hills, and S. Leslie, Overthrusting and sediment accretion along Kilauea's mobile south flank, Hawaii: Evidence for volcanic spreading from marine seismic reflection data, *Geology*, 28, 667–670, 2000.

Odonne, F., I. Ménard, G. J. Massonnat, and J. P. Rolando, Abnormal reverse faulting above a depleting reservoir, *Geology*, 27, 111–114, 1999.

Okubo, C. H., and S. J. Martel, Pit crater formation on Kilauea volcano, Hawaii, *J. Volcanol. Geotherm. Res.*, 86, 1–18, 1998.

Opheim, J. A., and A. Gudmundsson, Formation and geometry of fractures, and related volcanism, of the Krafla fissure swarm, northeast Iceland, *Geol. Soc. Am. Bull.*, 101, 1608–1622, 1989.

Peulvast, J.-P., D. Mège, J. Chiciak, F. Costard, and P. Masson, Origin and development of high-energy slopes in Valles Marineris (Mars); relations with tectonics and volatiles, *Geomorphology*, 37, 329–352, 2001.

Phillips, R. J., M. T. Zuber, S. C. Solomon, M. P. Golombek, B. M. Jakosky, W. B. Banerdt, D. E. Smith, R. M. E. Williams, B. M. Hynek, O. Aharonson, and S. A. Hauck II, Ancient geodynamics and global-scale hydrology of Mars, *Science*, 291, 2587–2591, 2001.

Platten, I. M., Incremental dilation of magma filled fractures: Evidence from dykes on the Isle of Skye, Scotland, *J. Struct. Geol.*, 22, 1153–1164, 2000.

Plescia, J. B., Graben and extension in northern Tharsis, Mars, *J. Geophys. Res.*, 96, 18,883–18,895, 1991.

Pollard, D. D., and G. Holzhausen, On the mechanical interaction between a fluid-filled fracture and the Earth's surface, *Tectonophysics*, 53, 27–57, 1979.

Pollard, D. D., P. T. Delaney, W. A. Duffield, E. T. Endo, and A. T. Okamura, Surface deformation in volcanic rift zones, *Tectonophysics*, 94, 541–584, 1983.

Reidel, S. P., T. L. Tolan, P. R. Hooper, M. H. Beeson, K. R. Fecht, R. D. Bentley, and J. L. Anderson, The Grande Ronde basalt, Columbia River Basalt Group; stratigraphic descriptions and correlations in Washington, Oregon, and Idaho, in *Volcanism and Tectonism in the Columbia River Flood-Basalt Province*, edited by S. P. Reidel and P. R. Hooper, *Geol. Soc. Am. Spec. Pap. 239*, 21–53, 1989.

Roche, O., T. Druitt, and O. Merle, Experimental study of caldera formation, *J. Geophys. Res.*, 105, 395–416, 2000.

Roche, O., B. van Wyk de Vries, and T. H. Druitt, Sub-surface structures and collapse mechanisms of summit pit craters, *J. Volcanol. Geotherm. Res.*, 105, 1–18, 2001.

Rubin, A. M., Dike-induced faulting and graben subsidence in volcanic rift zones, *J. Geophys. Res.*, 97, 1839–1858, 1992.

Rubin, A. M., Tensile fracture of rock at high confining pressure: Implications for dike propagation, *J. Geophys. Res.*, 98, 15,919–15,935, 1993.

Rubin, A. M., Propagation of magma-filled cracks, *Annu. Rev. Earth Planet. Sci.*, 23, 287–336, 1995.

Scheirer, D. S., and K. C. Macdonald, The variation in cross-sectional area of the axial ridge along the East Pacific Rise: Evidence for the magmatic budget of a fast-spreading center, *J. Geophys. Res.*, 98, 7871–7885, 1993.

Schultz, R. A., Do pit-crater chain grow up to be Valles Marineris canyons?, *NASA Tech. Memo.*, 4130, 539–540, 1988.

Schultz, R. A., Relative scale and the strength and deformability of rock masses, *J. Struct. Geol.*, 18, 1139–1149, 1996.

Schultz, R. A., Displacement-length scaling for terrestrial and Martian faults: Implications for Valles Marineris and shallow planetary graben, *J. Geophys. Res.*, 102, 12,009–12,015, 1997.

Schultz, R. A., Multiple-process origin of Valles Marineris basins and troughs, Mars, *Planet. Space Sci.*, 46, 827–834, 1998.

Schultz, R. A., Fault-population statistics at the Valles Marineris Extensional Province, Mars: Implications for segment linkage, crustal strains, and its geodynamical development, *Tectonophysics*, 316, 169–193, 2000.

Schultz, R. A., and A. N. Fori, Fault-length statistics and implications of graben sets at Candor Mensa, Mars, *J. Struct. Geol.*, 18, 373–383, 1996.

Schultz, R. A., and J. M. Moore, New observations of grabens from the Needles district, Canyonlands National Park, in *Geology and Resources*

of the Paradox Basin: Utah, edited by A. C. Huffman Jr., W. R. Lund, and L. H. Goodwin, *Geol. Assoc. Guideb.*, *25*, 295–302, 1996.

Schultz, R. A., J. A. Moore, E. B. Grosfils, K. L. Tanaka, D. Mège, E. Hauber, and P. Kronberg, Revised model for simple planetary graben and tectonic implications, *Lunar Planet. Sci. Conf.* [CD-ROM], *XXXI*, abstract 1175, 2000.

Scott D. H., and K. L. Tanaka , Geologic map of the western equatorial region of Mars, *U.S. Geol. Surv. Misc. Invest. Ser.*, *I-1802-A*, 1986.

Scott, E. D., L. Wilson, and J. W. Head III, Martian plinian eruptions and pit chain craters, *Lunar Planet. Sci. Conf.* [CD-ROM], *XXXI*, abstract 1332, 2000.

Sempere, J. C., and K. C. Macdonald, Overlapping spreading centers: Implications from crack growth simulation by the displacement discontinuity method, *Tectonics*, *5*, 151–163, 1986.

Shah, A. K., M.-H. Cormier, W. B. F. Ryan, W. Jin, J. Sinton, E. Bergmanis, J. Carlut, A. Bradley, and D. Yoerger, Episodic dike swarms inferred from near-bottom magnetic anomaly maps at the southern East Pacific Rise, *J. Geophys. Res.*, *108*(B2), 2097, doi:10.1029/2001JB000564, 2003.

Shaw, W. J., and J. Lin, Models of ocean ridge lithosphere deformation: Dependence on crustal thickness, spreading rate and segmentation, *J. Geophys. Res.*, *101*, 17,977–17,993, 1996.

Sinton, J., E. Bergmanis, K. Rubin, R. Batiza, T. K. P. Gregg, K. Grönvold, K. C. Macdonald, and S. M. White, Volcanic eruptions on mid-ocean ridges: New evidence from the superfast spreading East Pacific Rise, $17°–19°S$, *J. Geophys. Res.*, *107*(B6), doi:10.1029/2000JB000090, 2002.

Sleep, N. H., Martian plate tectonics, *J. Geophys. Res.*, *99*, 5639–5655, 1994a.

Sleep, N. H., Lithospheric thinning by midplate mantle plumes and the thermal history of hot plume material ponded at sublithospheric depths, *J. Geophys. Res.*, *99*, 9327–9343, 1994b.

Smith, D. E., et al., Mars Orbiter Laser Altimeter (MOLA): Experiment summary after the first year of global mapping of Mars, *J. Geophys. Res.*, *106*, 23,689–23,722, 2001.

Snyder, C. W., The missions of the Viking Orbiters, *J. Geophys. Res.*, *82*, 3971–3983, 1977.

Tanaka, K. L., Tectonic history of the Alba Patera-Ceraunius Fossae region of Mars, *Proc. Lunar Planet. Sci. Conf.*, *20th*, 515–523, 1990.

Tanaka, K. L., and P. A. Davis, Tectonic history of the Syria Planum province of Mars, *J. Geophys. Res.*, *93*, 14,893–14,917, 1988.

Tanaka, K. L., and M. P. Golombek, Martian tension fractures and the formation of graben and collapse features at Valles Marineris, *Proc. Lunar Planet. Sci. Conf.*, *19th*, 383–396, 1989.

Tanaka, K. L., M. P. Golombek, and W. B. Banerdt, Reconciliation of stress and structural histories of the Tharsis region of Mars, *J. Geophys. Res.*, *96*, 15,617–15,633, 1991.

Tazieff, H., The Erta' Ale volcano, *Rev. Geogr. Phys. Geol. Dyn.*, *15*, 437–441, 1973.

Thompson, R. N., and S. A. Gibson, Subcontinental mantle plumes, hot-spots and pre-existing thinspots, *J. Geol. Soc. London*, *148*, 973–977, 1991.

Turcotte, D. L., On the role of laminar and turbulent flow in buoyancy driven magma fractures, in *Magma Transport and Storage*, edited by M. P. Ryan, pp. 103–111, John Wiley, New York, 1990.

van Wyk de Vries, B., and O. Merle, The effect of volcanic constructs on rift fault patterns, *Geology*, *24*, 643–646, 1996.

Vendeville, B., P. R. Cobbold, P. H. Davy, J.-P. Brun, and P. Choukroune, Physicals models of extentional tectonics at various scales, in *Continental Extensional Tectonics*, edited by M. P. Coward, M. F. Dewey, and P. L. Hancock, *Geol. Soc. London Spec. Publ.*, *28*, 95–107, 1987.

Watters, T. R., Compressional tectonism on Mars, *J. Geophys. Res.*, *98*, 17,049–17,060, 1993.

Wilkins, S. J., and R. A. Schultz, Structural style and mode of extension in the northern Tempe rift, *Lunar Planet. Sci. Conf.* [CD-ROM], *XXXII*, abstract, 1253, 2001.

Wilson, L., and J. W. Head, Mars: Review and analysis of volcanic eruption theory and relationships to observed landforms, *Rev. Geophys.*, *32*, 221–263, 1994.

Wilson, L., and J. W. Head III, Tharsis-radial graben systems as the surface manifestation of plume-related dike intrusion complexes: Models and implications, *Lunar Planet. Sci. Conf.* [CD-ROM], *XXXI*, abstract 1371, 2000.

Wise, D. U., Faulting and stress trajectories near Alba volcano, northern Tharsis ridge of Mars, *Geol. Romana*, 430–433, 1976.

Wu, S. S. C., and F. J. Schafer, Mars control network, *Tech. Pap. Am. Soc. Photogramm.*, *50*, 456–463, 1984.

Yoerger, D. R., A. M. Bradley, B. B. Walden, M.-H. Cormier, and W. B. F. Ryan, Fine-scale seafloor survey in rugged deep-ocean terrain with an autonomous robot, paper presented at IEEE International Conference on Robotics Automation, Inst. of Electr. and Electr. Eng., San Francisco, Calif., 2000.

Zuber, M. T., The crust and mantle of Mars, *Nature*, *412*, 220–227, 2001.

Zuber, M. T., et al., Internal structure and early thermal evolution of Mars from Mars Global Surveyor topography and gravity, *Science*, *287*, 1788–1793, 2000.

————————————————

A. C. Cook, School of Computer Science and Information Technology, University of Nottingham, Jubilee Campus, Wollaton Road, Nottingham, NG8 1BB, UK. (acc@cs.nott.ac.uk)

M.-H. Cormier, Lamont-Doherty Earth Observatory, Columbia University, Palisades, NY 10964, USA. (cormier@ldeo.columbia.edu)

E. Garel, Laboratoire de Géodynamique des Rifts et des Marges Passives, Université du Maine, Avenue Olivier Messiaen, 72085 Le Mans Cedex 9, France. (Erwan.Garel@univ-lemans.fr)

Y. Lagabrielle, Institut de Recherche pour le Développement, CNRS UMR 6538, Université de Bretagne Occidentale, Place Nicolas Copernic, 29280 Plouzané, France. (yvesla@univ-brest.fr)

D. Mège, Laboratoire de Tectonique, CNRS UMR 7072, boîte 129, Université Pierre et Marie Curie, 4 Place Jussieu, 75252 Paris cedex 05, France. (dmege@lgs.jussieu.fr)